The influence of the pre-existing structuring on the evolution and geometry of extensional fault systems in the nothern North Sea rift system

Chao Deng

Thesis for the degree of philosophiae doctor (PhD)

at the University of Bergen

2017

Date of defence: 03.10.2017

博学之，审问之，慎思之，明辨之，笃行之。

--《礼记》

Erudite, questioning, deliberative, discerning and faithful.

Erudite, spørsmålet, deliberative, kresne og trofaste.

CONTENT

PREFACE

This thesis has been submitted for the degree of Doctor of Philosophy (Ph.D.) at the Department of Earth Science, University of Bergen, and has not previously been submitted for a degree in this or any other institutions. The work has been carried out at the University of Bergen, under the supervision of Prof. *Haakon Fossen*, Prof. *Robert Gawthorpe* and Prof. *Atle Rotevatn* at this university and two external co-supervisions of Dr *Emma Finch* at the University of Manchester and Prof. *Christopher Jackson* at Imperial College of London.

Following the guidelines of Norwegian doctoral dissertation in natural sciences, the main body of the thesis is composed of three research papers, which are prepared for submission to international, peer-reviewed geoscience journals. Paper I has been submitted to the *Marine and Petroleum Geology*. Paper II and Paper III are prepared for the *Journal of Structural Geology*. The format of the references in the three papers is thus in the format required for their respective journals. A general introduction about rationale, background and objectives of the work and the project in a broad view is given ahead of the three papers. Following the three papers, the thesis ends up with a synthesis chapter where the findings from the papers are integrated and discussed in the light of the problems outlined in the introduction from a broader perspective of the research.

ACKNOWLEDGEMENTS

First of all, I would like to thank my supervisors, *Haakon Fossen*, *Robert Gawthorpe* and *Atle Rotevatn* at the University of Bergen, for all their supervision, patience and support to me without reservation. I feel it is a privilege to have worked with and learned from all of you over the course of this Ph.D. project. It is your selfless dedication and continuous encouragement that makes me be able to overcome all the difficulties coming into my way during this work. I have learned a great lot from you, both in profession and life. Many thanks go to *Haakon*, who is a very nice and gentle person and who always with patience teaches me how to do research work and write a paper correctly. Also thank you, *Rob*, for your thoughtful ideas that make this work better and better after you comment on it again and again. Your brilliance and personal character is really admirable. Specially, I like to thank *Atle*, for your kindness and generosity to read and review my Paper I several times, even though you are not formally my supervisor. I am so thankful that you still spend time on helping me improving my manuscript. In a word, without your great contribution, I would not have made this work finished. Thank you for all your scientific guidance and inspiring discussion, and mostly important, for being so patient and humble all the time. And also thank you giving me this opportunity to co-work with and learn from you; your professionalism, experience and knowledge deeply arouse my interest in exploring the geologic world in my future life.

I am also grateful for my external supervisors *Emma Finch* and *Christopher Jackson*. Their input is a significant supplement for this work. *Emma* is a very smart lady who develops her own code to successfully simulate interesting geologic structures, providing a useful tool for learning and investigating on issues in structural geology. It is her effort in numerical modeling that makes this PhD project feasible. Thanks also for the contribution of *Chris*, for frequently asking my project progress and pushing me forward, in addition to your valuable reviews on the manuscript.

This project forms part of an inter-institutional “MultiRift Project”, and I thank all the

members of the project for the great discussion with them. Especially, I thank *Hamed Fazli Khani* for the numerous valuable discussions with you. You are so kind of offering me a great help while I interpret seismic data and write my thesis. And thank you for treating me as a young brother, giving me good suggestions in both scientific work and life. And I want to give my real appreciation to *Rosa Polanco-Ferrer*; she is great young lady and always so nice to talk to me, to tell me your colourful experience, and most importantly, to share delicious food with me. I wish our friendship will last forever. Also, I appreciate the help from the people at the Imperial College of London.

ABSTRACT

The structural style and fault evolution in rift basins affected by pre-existing structuring differ considerably from those developing above the homogeneous crust, because pre-existing structures are likely to reactivate and influence the fault network during subsequent rift phase(s) and result in the development of non-collinear faults. Most recent studies on the development of non-collinear faults have focused on the two-dimensional or three-dimensional geometries and the evolution of the fault network, as well as on the debate of extension directions. However, little attention has been given to how pre-existing structures reactivate and grow in three dimensions during the subsequent rift phase, and how they influence the fault geometries and fault network in the proximity.

The study contains two parts. The first part is the investigation of the geometry and evolution of normal fault systems of the Oseberg fault block in the northern North Sea which evolved over two separate rifting phases by interpreting seismic data (Paper I). The second part is the assessment of the fault growth pattern in three dimensions affected by a weak planar pre-existing structure during extension by discrete-element modeling (Papers II & III).

Three- and two-dimensional seismic and well data have been used to identify fault network of the Oseberg fault block in the northern North Sea – a rift system that experienced the Permian – Early Triassic and Middle Jurassic – Early Cretaceous rifting and exhibits N-S, NW-SE and NE-SW oriented faults. The N-S- and NW-SE-striking faults initiated during the Permian – Early Triassic rifting, and most of them reactivated during the Middle Jurassic – Early Cretaceous rifting, with an E-W extension direction. In contrast, the NE-SW-striking faults are of Middle Jurassic – Early Cretaceous origin. Moreover, a population of NW-SE-striking faults formed during the inter-rift phase, indicating a NE-SW inter-rift extension direction. The study suggests a reorientation of the stress field from E-W during the Permian – Early Triassic rift phase to NE-SW during the inter-rift fault growth and back to E-W during

the Middle Jurassic – Early Cretaceous rift phase in the Oseberg area. It also demonstrates that rift activity between established rift phases can locally develop faults with new orientations that add to the geometric and kinematic complexity of the final fault population.

Discrete element modelling has been used to investigate fault geometry and evolution of fault network in three dimensions above a weak planar pre-existing structure with various orientations relative to the extension direction and dips. The likelihood of reactivation reduces with either the orientation relative to extension direction or the dip of the pre-existing structure. Fully reactivated structure becomes a major fault, which decreases the density, changes the orientation, and enhances the displacement of adjacent faults. In contrast, the partly or little reactivated structure provides favorable sites for the nucleation of new faults. The evolution of the pre-existing weak structure and fault network is divided into three stages: (i) reactivation of pre-existing structure and nucleation of new faults; (ii) radial propagation and interaction between reactivated structure and new faults; and (iii) linkage between reactivated structure and adjacent faults. The modelling results suggest that the reactivation pattern of a pre-existing structure depends on both the orientation relative to extension direction and the dip, and influences the adjacent fault geometry and fault network via changing the fault density, length, orientation and displacement and providing favorable sites for fault nucleation.

The research demonstrates the complexity of final fault network as a result of the different reactivation style of the pre-existing structure and its influence on new fault growth. The study also contributes to the understanding of the reactivation pattern of a pre-existing structure as well as the evolution and geometries of fault interactions in three dimensions between the reactivated structure and newly formed faults. Lastly, the thesis also throws light on the control of the orientation of a pre-existing structure on the likelihood of reactivation and its subsequent role on adjacent fault network.

AUTHORSHIP STATEMENT

The topic of this PhD thesis was selected by the supervisors and the candidate together when the candidate started. The supervisors helped the candidate navigate the overall process and offered crucial suggestions and comments on the work over the course of this PhD project. The candidate was responsible for carrying out the research work and all the analysis performed based on the feedback of the supervisors, and is the first author of all three articles. The co-authors have provided lots of constructive comments, suggestions and advice while the candidate was drafting the papers. The detailed contributions of the supervisors to each paper are described below.

Paper I – Structural evolution during multiphase rifting: Oseberg area, northern North Sea

Chao Deng, Haakon Fossen, Robert L. Gawthorpe, Atle Rotevatn, Christopher A-L. Jackson, Hamed Fazli Khani

Marine and Petroleum Geology (submitted)

The candidate was responsible for interpretation and integration of the seismic and well data and for the geological analysis on interpretations. Haakon, Rob and Hamed guided the candidate to understand the geological issues and interpret the data in geologically correct and logical ways. The candidate wrote and drafted the manuscript at the first round. After that, Haakon, Rob, Atle, Chris and Hamed contributed to the review of the manuscript and input thoughtful discussions on presenting data and arguing effectively.

Paper II – Influence of pre-existing weakness on normal fault growth during an oblique extension: a case study by discrete element modeling

Chao Deng, Robert L. Gawthorpe, Haakon Fossen, Emma Finch

Journal of Structural Geology (manuscript in preparation)

Rob, Haakon and the candidate together worked out the model used for studying the influence of pre-existing weakness on normal fault growth. Emma constructed and run the numerical models at the University of Manchester by her own code of discrete

element modeling. The candidate was responsible for analysis and interpretation of the modeling results, wrote the manuscript and drafted all figures. Rob, Haakon and Emma engaged in discussion of the modelling results and revisions of the manuscript.

Paper III – How does the attitude of a pre-existing weakness influence fault development during renewed rifting? Some case studies by means of discrete element modeling

Chao Deng, Robert L. Gawthorpe, Haakon Fossen, Emma Finch

Journal of Structural Geology (manuscript in preparation)

A set of models were designed by Rob, Haakon and the candidate, in order to study the variability in the influence of pre-existing weakness on normal fault growth owing to the strike and dip. The numerical models were created and run by Emma on the super computer at the University of Manchester by means of a discrete element modeling code. The candidate was in charge of analyzing and interpreting the modeling results, wrote the manuscript and drafted all figures. Rob, Haakon and Emma engaged in discussion of the modeling result and the revision of the manuscript.

INTRODUCTION

1. Rationale

Rift basins are the result of crustal extension and thinning, characterized by brittle normal faulting in the upper crust and ductile flow in the lower crust (e.g. Mckenzie, 1978; Wernicke, 1985; Lister et al., 1986). The evolution and geometry of extensional fault systems in rift basins have been investigated globally, because they provide valuable information about (i) the geodynamic process of the crust and rift basins, and (ii) the kinematics of fault growth. Furthermore, the tectonic evolution of rift basins influence (iii) the balance of accommodation generation and sediment supply, which controls where and how much sediment is going to accumulate or be eroded, and essentially determines (iv) the locations, thickness and quality of reservoir-type sandstone. Moreover, the structural evolution of rift basins is also of importance for (v) understanding the formation of structural traps and hydrocarbon maturation and accumulation processes, which are critical elements of a petroleum system.

Many rift basins are influenced by pre-existing structures that exist in the basement of the rift system or form during an earlier phase of rifting, such as the North Sea rift system (Badley et al., 1988; Færseth, 1996; Odinsen et al., 2000; Whipp et al., 2014; Duffy et al., 2015), the Gulf of Aden (Lepvrier et al., 2002), the East African Rift System (Corti, 2012), Gulf of Thailand (Morley et al., 2004; Morley, 2007) and the North West Shelf, Australia (Frankowicz and McClay, 2010). Previous studies have mainly concentrated on fault geometries and fault network evolution based on interpretation of subsurface or field data (e.g., Færseth, 1996; Lepercq and Gaulier, 1996; Morley et al., 2004; Reston, 2005; Morley, 2007; Tomasso et al., 2008; Frankowicz and McClay, 2010; Bell et al., 2014; Duffy et al., 2015). However, our understanding of some of the key characteristics of pre-existing structures (e.g., reactivation pattern of pre-existing structures, impact of pre-existing structures on the development of adjacent new faults, growth of non-collinear faults) is rather poor, because the features associated with pre-existing structures become progressively

buried, tilted and structurally overprinted during subsequent rift phase(s) (e.g., Bell et al., 2014). Furthermore, the quality of subsurface data decreases with depth, which altogether makes it rather challenging to explore the structural features in such settings. As recent studies suggest that the geometry and structural evolution of many rift basins are largely influenced by pre-existing structures, it is important to improve our understanding of the impact of pre-existing structures on normal fault growth and development of such basins (e.g. Morley et al., 2004; Henza et al., 2010, 2011).

The purpose of this research is to investigate the three-dimensional fault geometries and structural evolution during rifting, with a focus on the reactivation pattern of first-phase faults during the second rift phase in the Oseberg area of the northern North Sea rift system. In more general terms, the research aims to understand the impact of reactivation of pre-existing structures on the development of newly-formed faults in the three-dimensional vicinity. The integrated results from this research give implications on the role of pre-existing structures on the final fault network and structural evolution of rift basins.

2. Background

2.1 Mechanisim of continental rifting

Continental rifts are areas of crustal stretching and thinning, and are generally associated with normal faulting and the development of rift basins in response to extension and tectonic subsidence (e.g. Gibbs, 1984, 1987; Lister et al., 1986; Withjack and Jamison, 1986; Rosendahl, 1987; Serra and Nelson, 1989; McClay, 1990; Nelson et al., 1992; Færseth, 1996; Bonini et al., 1997; McClay et al., 2002; Morley et al., 2004; Ziegler and Cloetingh, 2004; Bellahsen and Daniel, 2005; Huismans and Beaumont, 2007; Corti, 2012; Naliboff and Buiter, 2015). Traditionally, the initiation of crustal stretching and subsidence is assumed to fall into two end-members class (Sengör & Burke, 1978; Turcotte, 1983; Morgan & Baker, 1983; Keen, 1985; Bott, 1992): active and passive rifting (Fig. 1.1).

In active rifting, the stretching of the continental crust is the result of an active thermal process in the asthenosphere such as a mantle plume or sheet (Fig. 1.1a). Heat conducts and transfers from the mantle plume may cause thinning of the lithosphere, which promotes isostatic uplift of the lithosphere. Tensile stress is generated by the uplift (doming), and then followed by rifting. The East African and Ethiopian rifts have been explained in part in terms of active rifting (e.g. Ebinger, 2005; Agostini et al., 2009; Corti, 2009; Autin et al., 2010). In contrast, passive rifting involves the mechanical stretching of the continental crust from distant extensional forces (Fig. 1.1b). Upwelling of the underlying asthenosphere and rifting is therefore a passive response to a regional stress. During passive rifting, normal faulting precedes the thermal doming in the asthenosphere. The wide Basin and Range province of southwestern USA show evidence of passive rifting (e.g. Eaton, 1925; Zoback, 1989). However, it is not easy to determine whether a given rift is either active or passive. Natural rifts may exhibit elements of each model, since mantle uplift and regional stress field may promote each other during rifting (Khain, 1992). Huismans et al. (2001) observe a dynamic interplay between passive extension and active convective thinning of the mantle lithosphere beneath continental rift zones and suggest that the lithospheric horizontal stresses start to compete with the far-field intraplate stresses, and the doming forces may dominate and even drive the system from passive to active rifting.

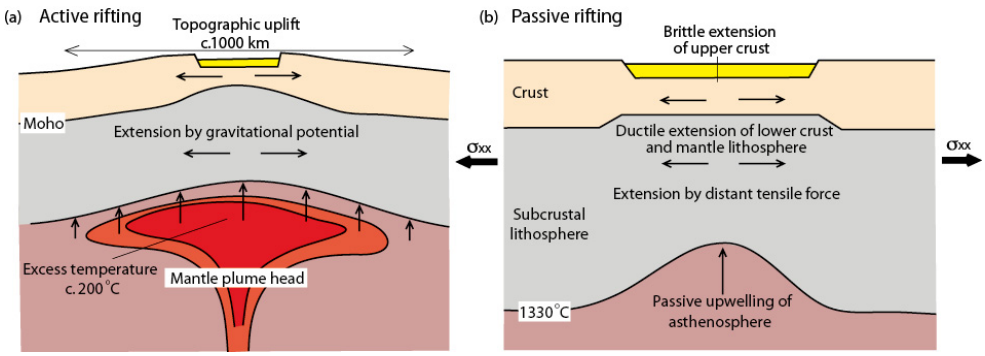

Figure 1.1 Two modes of rifting: a) active rifting due to occurrence of mantle plume, and b) passive rifting due to extension by distance tensile force (based on Allen and Allen, 2013).

2.2 Rift characteristics

Seismic studies show that continental rift zones are associated with crustal thinning (e.g. 16 km thick beneath the Viking Graben, while >30 km thick beneath the Shetland Platform and the Norwegian mainland). The crustal thickness depends on the stretching factor. The rift width is variable, ranging from 100 km (e.g., East African Rift System, Rio Grande Rift) to 1000 km (e.g., Basin and Range province of western USA). Typical characteristics of rift zones include (i) negative Bouguer gravity anomalies corresponding to the mass deficit of light basin sediment (e.g., East African Rift, Rosendahl, 1987; Ebinger and Ibrahim, 1994; Ziegler and Cloetingh, 2004) and (ii) high heat flow and volcanic activity owing to upwelling of hot material in the mantle and magmatic intrusion (e.g. Ebinger and Casey, 2001; Rogers, 2006; Yirgu et al., 2006). Furthermore, rift zones are featured by (iii) high levels of earthquake activity associated with active fault zones (e.g., Shudofsky et al., 1987; James and Tom, 1993) and (iv) a set of normal faults that are oriented perpendicular to the extension direction and mostly (but not necessarily) dipping basinward, with a variable percentage of strike-slip faults depending on the orientation rift axis relative to the extension direction (e.g., Gibbs, 1984; Bonini et al., 1997; McClay et al., 2002; Childs et al., 2003). Lastly, rift zones are typified by (v) the development of grabens or half-grabens controlled by basin-bounding faults (e.g., Gupta and Scholz, 2000; Cowie et al., 2000, 2005).

2.3 Evolution of rift basins and normal fault population

Cowie et al. (2005) presented a general model of fault evolution based on multi-scale observations of Middle-to-Late Jurassic extension of the northern North Sea: (i) a wide range of fault sizes formed during the extensional episode; (ii) present-day maximum fault throw increases towards rift axis; (iii) a preferred inward dip direction of large faults emerges as extension progressed and was accompanied by cessation of activity on outward dipping smaller-scale faults; (iv) maximum fault slip rate (or maximum strain rate) correlates with fault displacement (or β-stretching factor), as well as the duration of extension; and (v) the zone of active extension narrowed through time

(from ~200 km to <50 km over 40 Myr). This systematic migration of fault activity indicates that strain localization dominates basin development with strain rates at the eventual rift axis increasing and strain rates over flanking areas declining. Such progressive strain localization is not unique to the northern North Sea but can be observed in many modern rifts too, for example East Africa (Gupta and Scholz, 2000) and Gulf of Suez (Patton et al., 1994). Cowie et al. (2005) therefore suggest a coupling between near-surface strain localization, driven by brittle (or plastic) failure, and the evolving thermal structure of the lithosphere during the evolution of rift basins.

In terms of the evolution of a rift-related fault population during a single rift phase, a three-stage model is proposed based on field observations and numerical modeling: (i) initiation, (ii) interaction and linkage, and (iii) through-going fault zones (Fig. 1.2) (e.g., Trudgill and Cartwright, 1994; Cowie et al., 1995, 2000, 2005; Dawers and Anders, 1995; Dawers and Underhill, 2000; McLeod et al., 2000; Gawthorpe and Leeder, 2000; Childs et al., 2003). During the first stage, a great number of short and small-displaced normal fault segments initiate in the crust (Fig. 1.2a). Fault segments are isolated from each other, without interaction during this stage. During the second stage, the tips of fault segments propagate radially as strain accumulates. Stress feedback between segments influences their growth when the tips of fault segments come close. Following the linkage of segments, deformation begins to be localized along a few major fault zones (e.g. segments B and C in Fig. 1.2b). In contrast, the segments that are located in strain shadows become inactive (e.g. segment Z in Fig. 1.2b). During the through-going fault stage, deformation continues to be localized along major fault zones, resulting in the development of half-grabens and depocenters in the hanging walls of major faults (Fig. 1.2c).

2.4 Normal fault growth model

Normal fault growth is explained in terms of two end-member models: (i) the isolated fault model (Figure 1.3a) (e.g., Walsh and Watterson, 1988; Trudgill and Cartwright, 1994; Dawers and Anders, 1995; Cartwright et al., 1995; Schische and Anders, 1996,

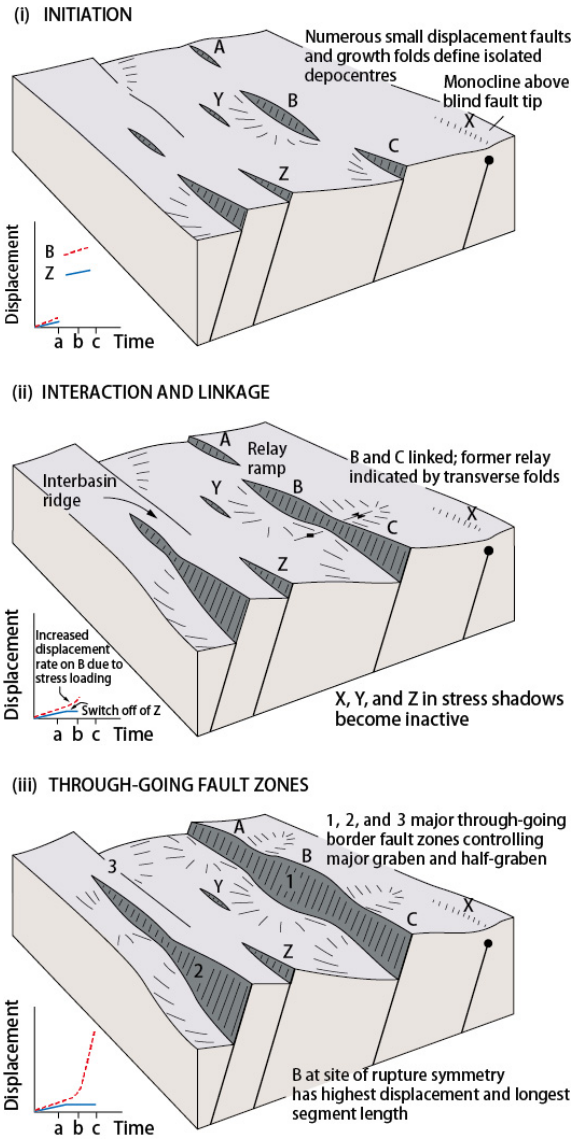

Figure 1.2: Schematic 3D evolution of a normal fault array, with graphs illustrating displacement history of fault segments B and Z. a) Fault initiation stage. b) Fault interaction and linkage stage. c) Through-going fault zone stage (modified after Gawthorpe and Leeder, 2000).

Contreras et al., 2000; McLeod et al., 2000; Mansfield and Cartwright, 2001; Young et al., 2001; Jackson et al., 2002; Walsh et al., 2002, 2003; Kim and Sanderson, 2005; Soliva et al., 2005; Baudon and Cartwright 2008); or (ii) the coherent fault model (Figure 1.3c, d) (e.g., Childs et al., 1995; Walsh et al., 2002, 2003; Schöpfer et al., 2006, 2007; Giba et al., 2012).

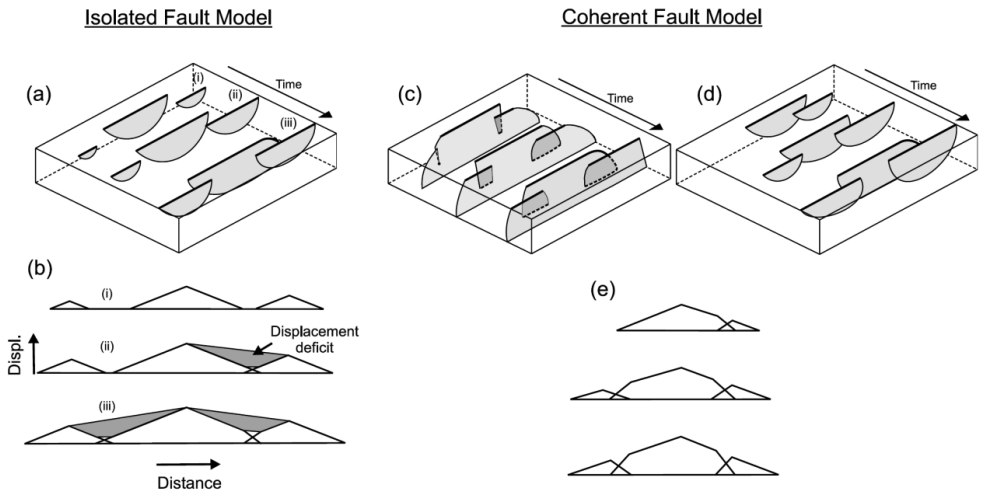

Fig. 1.3. Schematic illustrations of the two end-member models of formation of segmented fault arrays. The block diagrams (a, c and d) each show three stages in the growth of a segmented fault array (i–iii). The displacement-distance plots (b and e) are for the fault traces on the upper surfaces of the block diagrams (bold lines). The bold dashed lines in (c) indicate branch-lines. The shaded areas in (b) indicate deficits in displacement between the adjacent fault segments. (based on Walsh et al., 2003).

2.4.1 Isolated fault model

The isolated fault model describes the growth and eventual linkage of isolated fault segments via radial propagation of tip lines (e.g. Walsh and Watterson, 1988; Morley et al., 1990). This model suggests that extensional fault systems develop from a few individual segments, which then grow, link and amalgamate to form larger, continuous faults (Fig. 1.3a) (Cartwright et al., 1995; Gawthorpe and Leeder, 2000; Gawthorpe et

al., 1997; Mansfield and Cartwright, 2001; Peacock and Sanderson, 1991). As the individual faults laterally grow, overlap and interact, the displacement transfer is accommodated by relay zones (e.g. Peacock and Sanderson, 1994; Fossen and Rotevatn, 2016). Thus, individual fault segments develop displacement maximum at their center with displacement decreasing toward the tips, while linked faults are featured by several displacement maxima which represent the precursor fault strands separated by the linkage points where display displacement minimum (Fig. 1.3 b) (e.g. Gawthorpe and Leeder, 2000; Mansfield and Cartwright, 2001).

Fossen (2010) illustrated the growth of fault segments that propagate and link via the isolated fault model as a four-stage model: (i) fault initiation, (ii) fault overlap, (iii) fault interaction and, (iv) fault linkage (Fig. 1.4a). The displacement-length profiles during these stages show the temporal variation in the amount of slip (displacement) along the strike of the fault (Fig. 1.4b). During fault initiation (stage t_1), two isolated segments nucleate at different locations, with symmetric displacement-length profiles along strike. Following that, fault overlap occurs where the initial symmetric distribution of displacement will become asymmetric towards the interacting fault tips (stage t_2). Later (stage t_3), fault linkage will happen as a result of relay zone breaching. Finally, displacement distribution will become symmetric again (t_4), with further strain accumulation. Therefore, the shape of the displacement-length profile of a fault provides significant information about relative evolution of the fault in a fault population or array (Fossen, 2010). Also Peacock (2002) emphasized that the displacement-length relationship of normal faults is largely affected by interaction and linkage with adjacent faults. Especially, restriction between two faults during lateral propagation may result in a sharp decrease in displacement at the fault tips (e.g. Peacock and Sanderson, 1996; Peacock, 2002).

Therefore, isolated fault segments commonly grow by radial propagation, having the displacement maximum located in the middle of the segment (Fig. 1.3b), from where displacement decreases towards the tips (e.g., Walsh and Watterson, 1988; Cowie and Scholz, 1992; Dawers and Anders, 1993). This is the theoretical basis of using T-x plot

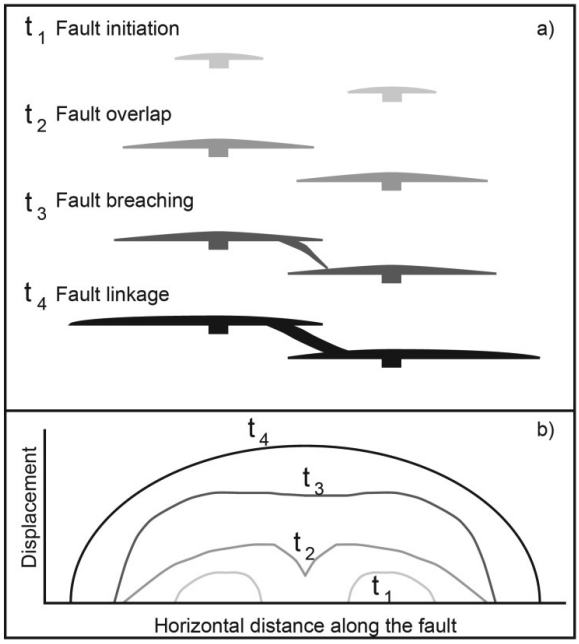

Figure 1.4. Normal fault linkage in a) plan-view and b) its associated displacement-length profile. At t1, two isolated normal faults grow. At t2, faults continue to grow and overlap and maximal displacement moves towards other overlapping fault. Faults interaction and linkage occurs at t3. At t4, fault is breached and linkage is finished and displacement-length profile is symmetric again (based on Fossen, 2010).

(Throw-distance) and T-z (Throw-depth) plots to reconstruct the growth history of a large fault system. Displacement maximum along the strike represents the nucleation point of fault segment, whereas displacement minimum shows the location of segment linkage (e.g., Childs et al., 1993, 1995; Ten Veen and Kleinspehn, 2000; Walsh et al., 2002; Taylor et al., 2004, 2008; Bell et al., 2014). In addition, Scholz et al., (1993) and Walsh et al. (2002) found that displacement maximum (D_{max}) and fault length (L) are related to each other by the formula $D_{max}=cL^n$, where c is a constant and n a scaling exponent. This scaling exponent is typically found to be around 1 to 1.5 for isolated normal fault (e.g., Walsh and Watterson, 1988; Cowie and Scholz, 1992; Dawers and Anders, 1995). Several normal fault data from natural examples have been collected and plotted in figure 1.5. The range of the exponent value, n, is from 0.5 to 2.0 (n=2.0,

Watterson, 1986; Walsh and Watterson, 1988; n=1.5, Marrett and Allmendinger, 1991; Gillespie et al., 1992; n=1, Cowie and Scholz, 1992; Dawers et al., 1993; Scholz et al., 1993; Schlische et al., 1996; n=0.5, Fossen and Hesthammer, 1997). The value of the exponent, n, is important as n=1 indicates a linear scaling law (i.e., self-similarity), and n≠1 is a scale-dependent geometry. The value of c is an expression of fault displacement at unit length. For a linear scaling (i.e., n=1), c is simply the ratio D_{max} /L.

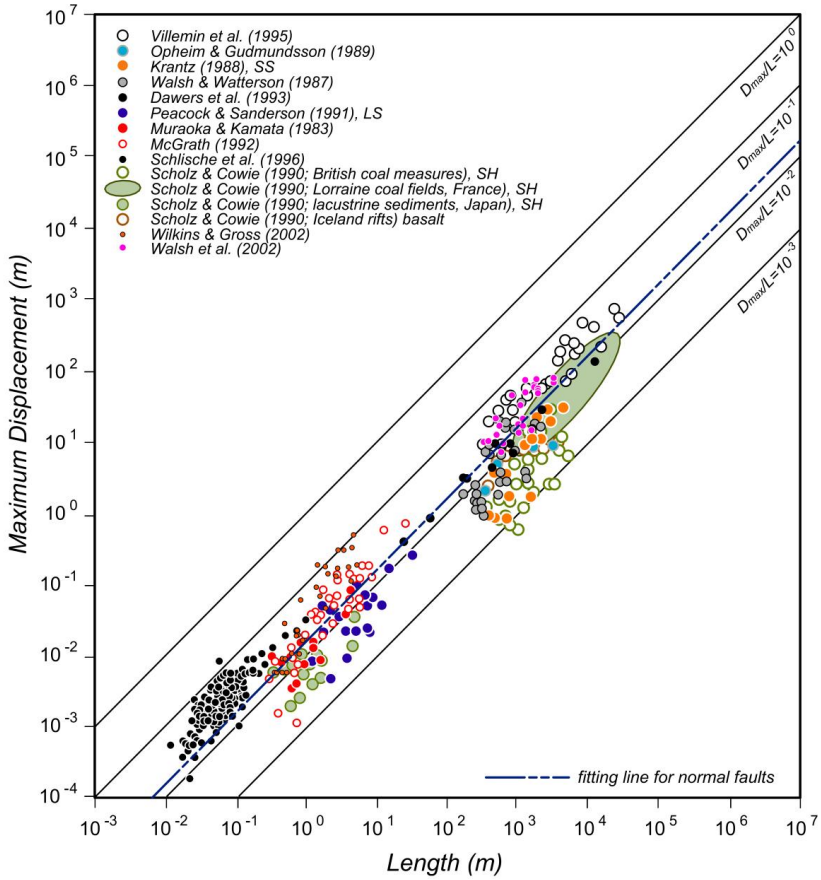

Fig. 1.5. Plots of maximum displacement (D_{max}) against fault length (L) (from Kim and Sanderson, 2005).

2.4.2 Coherent fault model

The coherent fault model, on the other hand, suggests that each fault segment initiates as a component of a spatially and mechanically related array (Fig. 1.3c, d) (e.g., Childs

et al., 1995; Walsh et al., 2002, 2003; Schöpfer et al., 2006, 2007; Giba et al., 2012). Subsequently, the fault segments are mainly featured by a gradual increase in displacement, without significant lateral propagation because of the interactions between adjacent segments. In addition, the coherent fault model assumes that faults splay vertically or laterally from a single fault surface into several fault segments (e.g., Walsh et al., 2002, 2003; Giba et al., 2012). Walsh et al. (2002, 2003) argued that the coherent fault model is particularly applicable to fault systems associated with reactivation of pre-existing structures. However, bifurcation of fault tips, and geometric and kinematic coherence of fault segments may also occur during a single phase of fault growth (e.g., Childs et al., 2003; Walsh et al., 2003; Schöpfer et al., 2006). Jackson and Rotevatn (2013) argued that the two growth models are not mutually exclusive, and may contribute, simultaneously, to the growth of a single fault.

The finite displacement distribution on segmented fault arrays in the coherent fault model differs from the isolated fault model. The aggregate displacement distribution gives a smooth and regular shape, with a displacement maximum in the middle, resembling that of a single isolated fault (Fig. 1.3e). In contrast, the aggregate displacement distribution in the isolated fault model will have several locations of displacement maxima, one located at the center of each fault segment (Fig. 1.3b). The different patterns of aggregate fault displacement distribution therefore provide the means for distinguishing between the basic end-member models for segmented faults (Fig. 1.3).

Walsh et al. (2002) argued that reactivated pre-existing faults are prone to evolve in coherent fault model and reach a near-final length in a very short period of the growth history, thus keeping a small value of displacement until further deformation progressively accumulates on it. Reactivation of pre-existing faults can therefore result in different D-L scaling relationships from the isolated fault model, with relative small displacement to length ratio (e.g. Gawthorpe and Leeder, 2000; Walsh et al. 2002). Bell et al. (2014) found that the D/L ratios for the Permian-Triassic Øy1, V1, and T1 fault systems in the northern North Sea are similar to those documented in southern

South Africa, which have demonstrably formed due to reactivation of pre-existing basement structures, and plot below the typical D/L gradient of n = 1, suggesting that they may be slightly under-displaced (Fig. 1.6).

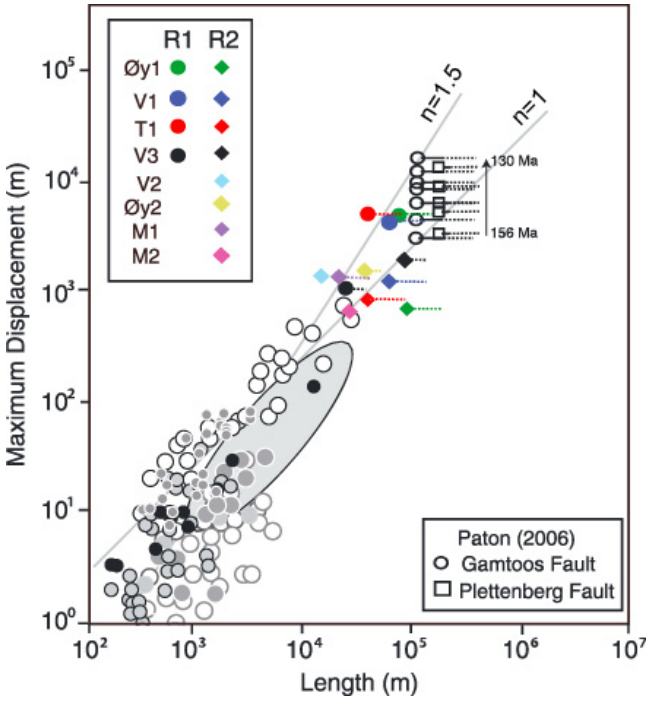

Fig. 1.6. Maximum displacement versus fault length plot using data from Kim and Sanderson (2005) (white, grey, and black circles on the left-hand side of the figure) and Paton (2006). Maximum displacement versus length measurements are shown for both faults following Rift Phase 1 (colored circles) and also following Rift Phase 2 (colored diamonds) (from Bell et al., 2014).

2.5 Fault growth in multiphase rifts

Multiphase rifts are rift zones that have experienced two or more phases of extension that are separated by a stage of tectonic quiescence dominated by post-rift thermal subsidence (e.g., the North Sea rift system, Gulf of Aden, East African Rift System, Gulf of Thailand and North West Shelf, Australia). Most studies about multiphase rifts have been conducted to analyze the fault geometries and fault interactions between

first-phase and second-phase faults by interpreting field (e.g., Strecker et al., 1990; Morley et al., 2004; Chan et al. 2010; Corti, 2012) and subsurface data (e.g., Færseth, 1996; Lepercq and Gaulier, 1996; Reston, 2005; Tomasso et al., 2008; Frankowicz and McClay, 2010; Bell et al., 2014; Duffy et al., 2015). In addition, physical (e.g., Keep and McClay, 1997; Henza et al., 2010, 2011) and numerical models (e.g., Roberts et al., 1995; Odinsen et al., 2000; Behn et al., 2002; Harry and Grandell, 2007; Naliboff and Buiter, 2015) are utilized to investigate the factors controlling the fault network and evolution during extension, such as change in extension direction (orthogonal vs. oblique), strain rate, rock strength and pre-existing structures. The following sections summarize the key findings of these different approaches.

2.5.1 Analysis of subsurface and field data

Previous studies by interpreting subsurface data and displacement distribution on faults provided very useful information about the fault interaction styles in three dimensions between first-phase and second-phase faults (Nixon et al., 2014; Duffy et al., 2015). The most common characteristic in a multiphase rift basin is that fault network is more complex than the basin with a single rift phase, with the development of fault populations having two or more different strikes. For example, the northern North Sea rift system experienced Permian-Early Triassic and Middle Jurassic-Early Cretaceous rifting and formed faults with three different strike directions: N-S, NW-SW and NE-SW, with the reactivation of first-phase faults and development of new faults during the second rift phase (e.g., Færseth, 1996; Færseth et al., 1997). In addition, fault interactions, such as abutting and crosscutting, happen between faults with different strikes, resulting in complex, non-collinear fault geometries (Fig. 1.7) (Duffy et al., 2015). Whipp et al. (2014) and Duffy et al. (2015) observed that first-phase N-S-striking faults were mostly reactivated as master faults and played a significant role in the distribution of strain during the second rift phase in the Horda Platform, northern North Sea. Hence, reactivation of pre-existing faults during a later rift phase and their interaction with second-phase faults is typical in the northern North Sea rift. Furthermore, Morley et al. (2004, 2007) found that first-phase faults are not

only reactivated during the second rift phase, but also have a great impact on the orientation of new faults developing close to them. These studies suggest that reactivation of pre-existing faults and the growth of new faults both happen during the second-phase of rifting, and these two fault populations are likely to interact with each other, adding complexities to the final fault network.

However, debates exist on the significance of the reactivation of first-phase faults and its influence on the fault growth during the second rift phase (Lee and Hwang, 1993; Thomas and Coward, 1995; Tomasso et al., 2008). Some authors utilizing high-quality 3D seismic reflection data in the East Shetland Basin in the northern North Sea argued that Triassic faults were largely crosscut and offset by oppositely dipping middle-late Jurassic faults, forming two generations of fault blocks tilted in opposite direction (Færseth et al., 1997; Færseth and Ravnas, 1998; Tomasso et al., 2008). Hence, considerable uncertainties still exist regarding to the degree and nature of fault reactivation during the second rift phase in the northern North Sea rift.

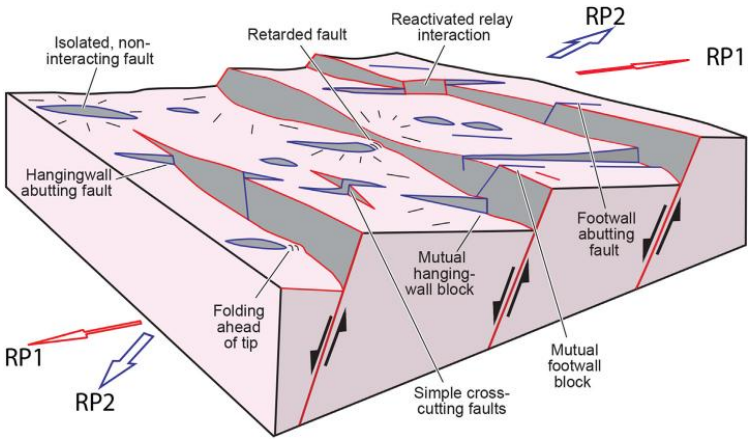

Fig. 1.7. Conceptual fault network model in a multiphase rift showing typical locations of, and styles of, interaction between non-colinear faults. The model assumes that the extension direction in rift phases 1 and 2 are different and that faults developed in rift phase 1 are reactivated during rift phase 2. RP1 = rift phase 1, resulting in the formation of faults outlined in red; RP2 = Rift Phase 2, resulting in faults outlined in blue (based on Duffy et al., 2015).

Also, our present understanding of some of the key and general characteristics during multiphase rifting (e.g., variation in the basin geometry, reactivation pattern of pre-existing structures and their impact on new fault growth) is rather limited, largely because the structural and stratigraphic features related to the first phase of extension become progressively deeper buried between and during individual rifting event (e.g., Bell et al., 2014). Even though subsurface data in multiphase rifts provide an excellent opportunity to investigate the tectono-stratigraphic evolution, rift structure and fault geometry in three dimensions (e.g., Steel and Ryseth, 1990; Faerseth, 1996; Odinsen et al., 2000; Tomasso et al., 2008; Frankowicz and McClay, 2010; Whipp et al., 2014), the availability of these data is restricted. Field data are more limited in nature, not only regarding to the scale of the outcrops compared to the full extent of the rift basin, but also the time span of the structure and stratigraphy relative to the multiple rift phases. Although these limitations do not exist in subsurface data acquired across hundreds of kilometers and data to depths of up to 10s of seconds (two-way time), their quality is the most critical problem, especially for the features associated with the earlier rift phases owing to the large depth and composite deformation history. Therefore, our understanding remains uncertain of the tectono-stratigraphic evolution and fault geometry related to the first-phase of rifting, as well as on how the pre-existing structures influence the subsequent rifting structures.

2.5.2 Physical analog modeling

Physical analog models have been employed to improve our insight into normal fault growth during multiphase extension with variable extension directions (e.g., Keep and McClay, 1997; Henza et al., 2010, 2011). For example, Henza et al. (2010, 2011) established a set of wet clay models and indicated that first-phase faults can be reactivated during the second phase of extension when the angle between first-phase faults and extension direction is less than ~45°. In addition to reactivation, the pre-existing structures can influence the nucleation and propagation of new faults around them, creating faults highly oblique to the extension direction and different styles of fault interactions (Henza et al. 2010, 2011). These physical analog models mainly

focus on specific factors controlling the fault development during non-coaxial multiphase rifting, such as the strength of pre-existing structure, the angle between extension directions, the magnitude of extension, etc. These parameters are proven to impact the rift characteristics of subsequent rifts including the fault geometry, evolution, orientation, sense of slip, and the number and location of new and reactivated faults (Bonini et al., 1997; Keep and McClay, 1997; Dubois et al., 2002; Morley et al., 2004; Bellahsen and Daniel, 2005; Henza et al., 2010, 2011). For example, the number and length of new fault segments increases together with the angle between the first- and second-phase extension directions (Dubois et al., 2002; Bellahsen and Daniel, 2005; Henza et al., 2010, 2011).

The advantages of using physical models to investigate a single or multiple phases of extension include that: (i) the scale of the models, extension directions and physical parameters can be manipulated to simulate a specific geological problem with a scale from a few kilometers to up to a few hundred kilometers; (ii) modeling results can be recorded through the process of modeling, displaying the structural evolution during extension; and (iii) modeling results can be compared with natural rifts, indicating what controls the evolution of multiphase rift basins. However, a major disadvantage is that most physical models only provide us with data from the surface of the models, rather than the real three-dimensional geometry inside the models. The truly three-dimensional fault geometries inside the models are critical for understanding fault growth and interactions. This limitation of physical modeling makes it unable to investigate the detailed three-dimensional growth pattern of normal faults and their effect on nearby normal faults inside models.

2.5.3 Numerical modeling

Numerical modeling is a method that incorporates the advantages of both subsurface data and physical modeling. Similar to subsurface data, numerical methods are able to provide detailed three-dimensional information, and a series of consecutive modeling results through the running process, just like physical models. For instance, discrete

element modeling has been successfully used to study crustal deformation during extension (e.g. Finch et al., 2004; Imber et al., 2004; Abe et al., 2011; Hardy et al, 2011). Finch et al. (2004) investigated the effect of overburden strength on the style of fault propagation folding above a blind normal fault, highlighting the suitability of discrete element modeling for studying crustal deformation and fault growth. In addition, Imber et al. (2004) used a three-dimensional discrete element model to study the evolution of a relay zone, which is considered a useful tool to reproduce the geometric and kinematic features seen in natural rifts and conceptual models by previous studies (e.g. Peacock and Sanderson, 1994; Childs et al., 1995; Walsh et al., 2002). More recently, Finch and Gawthorpe (2017) investigate the three-dimensional fault evolution and fault geometry in homogeneous material during single-phase rifting by using discrete element modeling, which gives a better insight into the nucleation, propagation and linkage of a fault system during single-phase rifting. The modeling results indicate that the T-x and T-z plots commonly used to analyze the history of fault nucleation, propagation and linkage, are not everywhere applicable as the throw maximum can migrate from one place to another during extension.

Another advantage of numerical modeling is the ability to solve lithospheric-scale problems, such as the effect of the lithospheric thermal structure on the development of rift basins (e.g., Cowie et al., 2005). Several numerical models of multiphase extensions focused on the tectonic influence of lithosphere structures on the subsequent rift development, including the size of thermal perturbation (e.g., Odinsen et al., 2000), pre-existing weakness in the lithosphere (e.g., Harry and Grandell, 2007) and lithospheric strengthening (e.g., Reemst and Cloetingh, 2000). Behn et al. (2002) used finite element modeling to investigate the significance of lithosphere rheology and thermal structure on normal fault growth in extensional settings. They found that rift-like topography with focused normal faulting forms in response to a horizontally varying thermal structure in the lithosphere, while distributed deformation on several sets of conjugate normal faults develop in response to constant regional temperature. In contrast, Huismans and Beaumont (2007) examined the effect of lithospheric strain softening and pre-existing heterogeneities on the geometry of rifts by using thermos-

mechanical finite modeling. Altogether, these numerical models aim to understand the dynamic mechanism of the development of rift system and basins in the lithospheric scale.

3. Aim and objective

The overall aim of this study is to improve our understanding of the influence of pre-existing faults or structures on the development of newly formed faults during rifting in three dimensions. The influence of pre-existing faults or structure in three dimensions is of great importance for understanding (i) the reactivation and growth pattern of a pre-existing fault or structure; (ii) the final fault network affected by a pre-existing fault or structure, such as the development of non-collinear faults and variation in three-dimensional fault geometries; and (iii) different styles of fault interactions and their growth process; and finally (iv) strain localization and structural evolution of multiphase rifts.

The research is divided into two parts: one is to examine the structural evolution and fault growth history of the Oseberg area, norther North Sea by analysis of subsurface data (**Paper I**); the other is to investigate the reactivation pattern of a pre-existing weak structure and its influence on new fault growth during extension by discrete element modeling (**Papers II & III**). The specific objectives include:

1. Understanding the control of fault evolution during the multiphase rifting and the significance of pre-existing structure to final fault geometry and fault network (**Paper I**).
2. Investigating how a planar pre-existing structure (or weakness) reactivates and then propagates at a chosen strike angle of 60° to extension direction, and how it influences the growth and geometry of new faults developing in its proximity (**Paper II**).
3. Examining the control of the strike and dip of a weak planar pre-existing structure relative to extension direction on the variations in the reactivation

pattern of the pre-existing structure and its following impact on new fault growth during extension (**Paper III**).

The brief summary of the three papers is present below.

SUMMARY

Paper I – Influence of fault reactivation during multiphase rifting: the Oseberg area, Northern North Sea rift

Chao Deng, Haakon Fossen, Robert L. Gawthorpe, Atle Rotevatn, Christopher A-L. Jackson, Hamed FazliKhani

Marine and Petroleum Geology (under review)

This paper discusses the role of pre-existing faults and change in extension direction on the fault network and structure evolution in the Oseberg area, norther North Sea. The work is based on interpreting 3D seismic data and 2D transects, which is calibrated by numerous wells. Horizons and faults related to both the Permian – Early Triassic and the Middle Jurassic – Early Cretaceous rift phases are interpreted to investigate the fault geometries and fault evolution in the study area.

Faults exhibit N-S, NW-SE and NE-SW orientations. Both N-S- and NW-SE-striking faults were established during the Permian – Early Triassic rifting, as indicated by Triassic growth packages in their hanging walls. The NE-SW-striking faults initiated during Middle Jurassic – Early Cretaceous rifting because they only show evidence of Middle Jurassic – Early Cretaceous growth, and offset several N-S- and NW-SE-striking faults. We also identify the inter-rift activity during the time period between the two rift phases based on the growth packages in the hanging walls of a set of NW-SE-striking faults, indicating a NE-SW inter-rift extension direction. Faults initiated during the Permian – Early Triassic and Middle Jurassic – Early Cretaceous rift phases show mainly N-S orientation, indicating E-W extension during the two rift phases.

These observations suggest a reorientation of the stress field from E-W during the Permian – Early Triassic rift phase to NE-SW during inter-rift fault growth and back to E-W during the Middle Jurassic – Early Cretaceous rift phase in the Oseberg area. Reactivation of the Permian – Early Triassic faults happens during the Middle Jurassic – Early Cretaceous rift phase. As the end, a generic model of four styles of the renewed growth of a reactivated fault is proposed.

Paper II – Influence of pre-existing weakness on normal fault growth during an oblique extension: a case study by discrete element modeling

Chao Deng, Robert L. Gawthorpe, Emma Finch, Haakon Fossen

Journal of Structural Geology (manuscript in preparation)

This paper utilizes discrete element modeling to investigate the influence of a weak planar pre-existing structure on the growth of newly formed faults in its proximity during extension. Faults and horizons related to the pre-existing structure and adjacent new faults are extracted from the early to late stages of the extension. The main purpose focus on fault geometry, fault interaction and the evolution of the fault network in three dimensions above the weak planar pre-existing structure striking at 60° to the extension direction and dipping at 60°.

Fault network evolution affected by a weak planar pre-existing structure is summarized in three stages: (i) reactivation of pre-existing structure and nucleation of new faults (0-10% extension); (ii) radial propagation and interaction between the reactivated structure and new faults (15%-20% extension); and (iii) linkage between the reactivated structure and adjacent faults (20%-25% extension). The reactivation pattern and further growth of the pre-existing structure is illustrated in detail, with respect to the fault length, strike, tip line and fault displacement. Our modeling results show that the pre-existing structure forms a long and under-displaced fault early in its growth history, followed by a long period of displacement accumulation. The upward propagation of the reactivated structure is featured by a few ‘saw-tooth’ fringes at upper tip. In addition, the effect of the reactivated structure on new fault growth in its

vicinity is manifested in terms of the variation in the number, orientation and displacement of adjacent new faults. Furthermore, four styles of fault interactions are recognized between the reactivated structure and adjacent new faults and the evolution of each fault interaction style is exhibited in three dimensions. This work indicates that a reactivated structure propagates in an irregular ('saw-tooth') pattern, and influences the geometry and distribution of new faults in its proximity by changing fault density, orientation and displacement.

Paper III – How does the attitude of a pre-existing weakness influence fault development during renewed rifting? Some case studies by discrete element modeling

Chao Deng, Robert L. Gawthorpe, Haakon Fossen, Emma Finch

Journal of Structural Geology (manuscript in preparation)

This paper continues using discrete element modeling to investigate the influence of a pre-existing weak planar structure on the fault geometry, fault interaction and the evolution of the fault network in three dimensions in its proximity during extension. On the basis of the Paper II, the main purpose here is to investigate the varieties in the likelihood of reactivation of a pre-existing fault and styles of fault interaction in three dimensions, with respect to a variable angle (30°-90°) of the orientation relative to extension direction and dip (30°-60°) of the pre-existing planar structure.

The geometry of the pre-existing structure at different stages of extension is illustrated in three dimensions, including the fault length, strike, tip line and fault displacement. The modeling results show that the reactivation of a pre-existing weak structure has three types: (i) full reactivation if it has a large angle (≥60°) to the extension direction and dips steeply (60°); (ii) partial reactivation if it has a moderate angle (45°) to the extension direction or a moderate dip (45°); and (iii) no or little reactivation if it has a small angle (30°) to the extension direction or small dip (30°). In addition, there are more chance of fault interactions such as abutting and twisting when the pre-existing structure fully or partly reactivates, but more possibility of crosscutting when the pre-

existing structure is inactive. Our study suggests that the reactivation pattern of a pre-existing structure and its influence on new fault growth depends on both its orientation relative to extension direction and dip. It also implies that a pre-existing structure influences the adjacent fault geometry and fault network by changing the fault density, length, orientation and displacement and by providing favorable sites for fault nucleation.

Reference

Abe, S., Van Gent, H., & Urai, J. L., 2011, DEM simulation of normal faults in cohesive materials, Tectonophysics, 512, 12-21.

Agostini, A., Corti, G., Zeoli, A., Mulugeta, G., 2009. Evolution, pattern and partitioning of deformation during oblique continental rifting: inferences from lithospheric-scale centrifuge models. Geochemistry, Geosphysics, Geosystems (GCubed) 10, Q11015.

Autin, J., Bellahsen, N., Husson, L., Beslier, M.O., Leroy, S., d'Acremont, E., 2010. Analogue models of oblique rifting in a cold lithosphere. Tectonics 29, TC6016.

Badley, M., Price, J., Dahl, C.R., Agdestein, T., 1988. The structural evolution of the northern Viking Graben and its bearing upon extensional modes of basin formation. Journal of the Geological Society 145, 455-472.

Baudon, C., and Cartwright, J., 2008, Early stage evolution of growth faults: 3D seismic insights from the Levant Basin, Eastern Mediterranean, Journal of Structural Geology, 30, 888-898.

Behn, M. D., Lin, J. and Zuber, M. T., 2002, A continuum mechanics model for normal faulting using a strain-rate softening rheology: implications for thermal and rheological controls on continental and oceanic rifting, Earth and Planetary Science Letters, 202, 725-740.

Bell, R. E., Jackson, C. A-L., Whipp, P. S., and Clements, B., 2014, Strain migration during multiphase extension: Observations from the northern North Sea, Tectonics, 33, 1936-1963.

Bellahsen, N., and Daniel, J. M., 2005, Fault reactivation control on normal fault growth: an experimental study, Journal of Structural Geology, 27, 769-780.

Bonini, M., Souriot, T., Boccaletti, M., and Brun, J. P., 1997, Successive orthogonal and oblique extension episodes in a rift zone: Laboratory experiments with application to the Ethiopian Rift, Tectonics, 16, 347-362.

Bott, M.H.P., 1992. Modelling the loading stresses associated with active continental rift systems. Tectonophysics, 215, 99–115.

Cartwright, J. A., Bouroullec, R., James, D., and Johnson, H. D., 1998, Polycyclic motion history of some Gulf Coast growth faults from high-resolution displacement analysis, Geology, 26, 819-822.

Cartwright, J. A., Trudgill, B. D., & Mansfield, C. S. 1995, Fault growth by segment linkage: an explanation for scatter in maximum displacement and trace length data from the Canyonlands Grabens of SE Utah, Journal of Structural Geology, 17, 1319-1326.

Chan, L. S., Shen, W., and Pubellier, M., 2010, Polyphase rifting of greater Pearl River Delta region (South China): Evidence for possible rapid changes in regional stress configuration, Journal of Structural Geology, 32, 746-754.

Childs, C., A. Nicol, J. J. Walsh, and J. Watterson, 2003, The growth and propagation of synsedimentary faults, J. Struct. Geol., 25, 633-648.

Childs, C., Easton, S. J., Vendeville, B. C., Jackson, M. P. A., Lin, S. T., Walsh, J. J., & Watterson, J., 1993, Kinematic analysis of faults in a physical model of growth faulting above a viscous salt analogue, Tectonophysics, 228, 313-329.

Childs, C., Watterson, J., and Walsh, J. J., 1995, Fault overlap zones within developing normal fault systems, Journal of the Geological Society, London, 152, 535-549.

Contreras, J., Anders, M. H., & Scholz, C. H, 2000, Growth of a normal fault system: observations from the Lake Malawi basin of the east African rift, Journal of Structural Geology, 22, 159-168.

Corti, G., 2009. Continental rift evolution: from rift initiation to incipient break-up in the Main Ethiopian Rift, East Africa. Earth Science Reviews 96, 1–53.

Corti, G., 2012, Evolution and characteristics of continental rifting: Analog modeling inspired view and comparison with examples from the East African Rift System, Tectonophysics, 522-523, 1-33.

Cowie, P. A., and Scholz, C. H., 1992, Physical explanation for the displacement-length relationship of faults using a post-yield fracture mechanics model, Journal of Structural Geology, 14, 1133-1148.

Cowie, P. A., Sornette, D., and Vanneste, C., 1995. Multifractal scaling properties of a growing fault population, Geophysical Journal International, 122, 457-469.

Cowie, P. A., Underhill, J. R., Behn, M. D., Lin, J., and Gill, C. E., 2005, Spatio-temporal evolution of strain accumulation derived from multi-scale observations of Late Jurassic rifting in the northern North Sea: A critical test of models for lithospheric extension, Earth and Planetary Science Letters, 234, 401-419.

Cowie, P., Gupta, S., Dawers, N., 2000. Implications of fault array evolution for synrift depocentre development: insights from a numerical fault growth model. Basin Research 12, 241-261.

Dawers, N. H., and Anders, M. H., 1995, Displacement-length scaling and fault linkage Journal of Structural Geology, 17, 607-614.

Dawers, N. H., and J. R. Underhill, 2000, The role of fault interaction and linkage in controlling syn-rift stratigraphic sequences: Statfjord East area, northern North Sea, AAPG Bulletin, 84, 45-64.

Dawers, N. H., Anders, M. H., and Scholz, C. H., 1993, Growth of normal faults: Displacement-length scaling, Geology, 21, 1107-1110.

Dubois, A., Odonne, F., Massonnat, G., Lebourg, T., and Fabre, R., 2002, Analogue modelling of fault reactivation: tectonic inversion and oblique remobilization of grabens, Journal of Structural Geology, 24, 1741-1752.

Duffy, O.B., Bell, R.E., Jackson, C.A., Gawthorpe, R.L., Whipp, P.S., 2015. Fault growth and interactions in a multiphase rift fault network: Horda Platform, Norwegian North Sea. Journal of Structural Geology 80, 99-119.

Eaton, G. P., 1925. The basin and range province: origin and tectonic significance. Annual Review of Earth & Planetary Sciences, 10(1), 409-440.

Ebinger, C., Casey, M., 2001. Continental breakup in magmatic provinces: an Ethiopian example. Geology, 29, 527–530.

Ebinger, C. J., & Ibrahim, A., 1994. Multiple episodes of rifting in Central and East Africa: A re-evaluation of gravity data. Geologische Rundschau, 83(4), 689-702.

Færseth, R. B., & Ravnås, R., 1998. Evolution of the oseberg fault-block in context of the northern North Sea structural framework. Marine & Petroleum Geology, 15(5), 467-490.

Færseth, R., 1996. Interaction of Permo-Triassic and Jurassic extensional fault-blocks during the development of the northern North Sea. Journal of the Geological Society 153, 931-944.

Færseth, R.B., Knudsen, B.E., Liljedahl, T., Midbøe, P.S., Søderstrøm, B., 1997. Oblique rifting and sequential faulting in the Jurassic development of the northern North Sea. Journal of Structural Geology 19, 1285-1302.

Finch, E., Hardy, S., & Gawthorpe, R. L., 2004, Discrete□element modelling of extensional fault propagation folding above rigid basement fault blocks, Basin Research, 16, 467-488.

Fossen, H., Hesthammer, J., 1997. Geometric analysis and scaling relations of deformation bands in porous sandstone. Journal of Structural Geology 19, 1479– 1493.

Fossen, H., 2010, Structural Geology, New York, Cambridge University Press, 463.

Fossen, H., & Rotevatn, A., 2016. Fault linkage and relay structures in extensional settings—a review. Earth-Science Reviews, 154, 14-28.

Frankowicz, E., McClay, K., 2010. Extensional fault segmentation and linkages, Bonaparte Gawthorpe, R., Leeder, M., 2000. Tectono-sedimentary evolution of active extensional basins. Basin Research 12, 195-218.

Gawthorpe, R. L., and Leeder, M. R., 2000, Tectono-sedimentary evolution of active extensional basins, Basin Research, 12, 195-218.

Gawthorpe, R. L., Sharp, I., Underhill, J. R., & Gupta, S., 1997, Linked sequence stratigraphic and structural evolution of propagating normal faults, Geology, 25, 795-798.

Giba, M., Walsh, J. J., and Nicol, A., 2012, Segmentation and growth of an obliquely reactivated normal fault, J. Struct. Geol., 39, 253-267.

Gibbs, A. D., 1984, Structural evolution of extensional basin margins, J. Geol. Soc. London, 141, 609-620.

Gibbs, A. D., 1987, Development of extension and mixed-mode sedimentary basins, In: Coward, M. P., Dewey, J. F., and Hancock, P. L. (eds), Continental Extensional Tectonics, Geological Society Special Publicatios, 28, 19-33.

Gillespie, P.A., Walsh, J.J., Watterson, J., 1992. Limitations of dimension and displacement data from single faults and the consequences for data analysis and interpretation. Journal of Structural Geology 14, 1157– 1172.

Gupta, A., Scholz, C.H., 2000, Brittle strain regime transition in the Afar depression: implications for fault growth and seafloor spreading, Geology 28 1087–1090.

Hardy, S., 2011, Cover deformation above steep, basement normal faults: Insights from 2D discrete element modeling, Marine and Petroleum geology, 28, 966-972.

Harry, D. L., and Grandell, S., 2007, A dynamic model of rifting between Galicia Bank and Flemish Cap during the opening of the North Atlantic Ocean, Geological Society, London, Special Publications, 282, 157-172.

Henza, A.A., Withjack, M.O., Schlische, R.W., 2010. Normal-fault development during two phases of non-coaxial extension: An experimental study. Journal of Structural Geology 32, 1656-1667.

Henza, A.A., Withjack, M.O., Schlische, R.W., 2011. How do the properties of a pre-existing normal-fault population influence fault development during a subsequent phase of extension? Journal of Structural Geology 33, 1312-1324.

Huismans, R. S., Beaumont, C. 2007, Roles of lithospheric strain softening and heterogeneity in determining the geometry of rifts and continental margins, Geol. Soc. London Spec. Publ., 282, 111-138.

Huismans, R. S., Podladchikov, Y. Y. and Cloetingh, S. A. P. L., 2001, The transition from passive to active rifting, relative importance of asthenospheric doming and passive extension of the lithosphere, Journal of Geophysical Research, 106, 11,271-11,291.

Imber, J., Tuckwell, G. W., Childs, C., Walsh, J. J., Manzocchi, T., Heath, A. E., Bonson, C. G., & Strand, J., 2004, Three-dimensional distinct element modelling of relay growth and breaching along normal faults, Journal of Structural Geology, 26, 1897-1911.

Jackson, C. A-L., and Rotevatn, A., 2013, 3D seismic analysis of the structure and evolution of a salt-influenced normal fault zone: a test of competing fault growth models, J. Struct. Geol. 54, 215-234.

Jackson, C. A-L., Gawthorpe, R. L., & Sharp, I. R., 2002, Growth and linkage of the East Tanka fault zone, Suez rift: structural style and syn-rift stratigraphic response, Journal of the Geological Society, 159, 175-187.

James, J., & Tom, B., 1993. The malawi earthquake of march 10, 1989: deep faulting within the east african rift system. Tectonics, 12(5), 1131-1139.

Keen, C.E., 1985. The dynamics of rifting: deformation of the lithosphere by active and passive driving forces. Geophysical Journal of the Royal Astronomical Society, 80, 95–120.

Keep, M., and McClay, K.R., 1997, Analogue modelling of multiphase rift systems, Tectonophysics, 273, 239-270.

Khain, V.Y., 1992. The role of rifting in the evolution of the Earth's crust. Tectonophysics, 215, 1–7.

Kim, Y. S., & Sanderson, D. J., 2005, The relationship between displacement and length of faults: a review, Earth-Science Reviews, 68, 317-334.

Lee, M. J., and Hwang, Y. J., 1993, Tectonic evolution and structural styles of the East Shetland Basin, Petroleum Geology of Northwest Europe: Proceedings of the 4th Conference, 1137-1149.

Lepercq, J. Y., and Gaulier, J. M., 1996, Two-stage rifting in the North Viking Graben area (North Sea): inferences from a new three-dimensional subsidence analysis, Marine and Petroleum Geology, 13, 129-148.

Lepvrier, C., Fournier, M., Bérard, T., Roger, J., 2002. Cenozoic extension in coastal Dhofar (southern Oman): implications on the oblique rifting of the Gulf of Aden. Tectonophysics 357, 279-293.

Lister, G. S., Etherdge, M. A., and Symonds, P. A. 1986, Detachment faulting and the evolution of passive continental margins, Geology, 14, 246-250.

Mansfield, C., & Cartwright, J., 2001, Fault growth by linkage: observations and implications from analogue models, Journal of Structural Geology, 23, 745-763.

Marrett, R., Allmendinger, R.W., 1991. Estimates of strain due to brittle faulting: sampling of fault populations. Journal of Structural Geology 13, 735–738.

McClay, K. R., 1990, Extensional fault systems in sedimentary basins: a review of analogue model studies, Marine and Petroleum Geology, 7, 206-233.

McClay, K. R., Dooley, T., Whitehouse, P., and Mills, M., 2002, 4-D evolution of rift systems: Insights from scaled physical models, AAPG Bulletin, 86, 935-960.

McKenzie, D., 1978, Some remarks on the development of sedimentary basins, Earth and Planetary Science Letters, 40, 25-32.

McLeod, A. E., Dawers, N. H., and Underhill, J. R., 2000, The propagation and linkage of normal faults: Insights from the Strathspey–Brent–Statfjord fault array, northern North Sea, Basin Research, 12, 263-284.

Morgan, P. and Baker, B.H., 1983. Introduction: processes of continental rifting. Tectonophysics, 94, 1–10.

Morley, C. K., Nelson, R. A., Patton, T. L. & Munn, S. G. 1990. Transfer zones in the East African rift system and their relevance to hydrocarbon exploration in rifts. Bull. Am. Ass. Petrol. Geol. 74, 1234-1253.

Morley, C., Gabdi, S., Seusutthiya, K., 2007. Fault superimposition and linkage resulting from stress changes during rifting: Examples from 3D seismic data, Phitsanulok Basin, Thailand. Journal of Structural Geology 29, 646-663.

Morley, C., Haranya, C., Phoosongsee, W., Pongwapee, S., Kornsawan, A., Wonganan, N., 2004. Activation of rift oblique and rift parallel pre-existing fabrics during extension and their effect on deformation style: examples from the rifts of Thailand. Journal of Structural Geology 26, 1803-1829.

Naliboff, J., and Buiter, S.J.H., 2015, Rift reactivation and migration during multiphase extension, Earth and Planetary Science Letters, 421, 58-67.

Nelson, R. A., Patton, T. L., and Morley, C. K., 1992, Rift-segment interaction and its relation to hydrocarbon exploration in continental rift systems, AAPG Bulletin, 76, 1153-1169.

Nixon, C. W., Bull, J. M., & Sanderson, D. J., 2014, Localized vs distributed deformation associated with the linkage history of an active normal fault, Whakatane Graben, New Zealand, Journal of Structural Geology, 69, 266-280.

Odinsen, T., Reemst, P., Beek, P.V.D., Faleide, J.I., Gabrielsen, R.H., 2000. Permo-Triassic and Jurassic extension in the northern North Sea: results from tectonostratigraphic forward modelling. Geological Society, London, Special Publications 167, 83-103.

Paton, D. A., 2006. Influence of crustal heterogeneity on normal fault dimensions and evolution: Southern South Africa extensional system, J. Struct. Geol., 28, 868–886.

Patton T.L., Moustafa A.R., Nelson R.A., Abdine S.A., 1994. Tectonic evolution and structural setting of the Suez Rift, in: S. Landon (Ed.), Interior Rift Basins, AAPG Mem., vol. 59, pp. 9– 55.

Peacock, D. C. P., & Sanderson, D. J., 1994, Geometry and development of relay ramps in normal fault systems, AAPG bulletin, 78, 147-165.

Peacock, D. C. P., & Sanderson, D. J., 1996, Effects of propagation rate on displacement variations along faults, Journal of Structural Geology, 18, 311-320.

Peacock, D. C. P., 2002. Propagation, interaction and linkage in normal fault systems. Earth-Science Reviews, 58(1–2), 121-142.

Peacock, D. C. P., and Sanderson, D. J., 1991, Displacements, segment linkage and relay ramps in normal-fault zones, Journal of Structural Geology, 13, 721-733.

Reemst, P., & Cloetingh, S., 2000. Polyphase rift evolution of the vøring margin (mid - norway): constraints from forward tectonostratigraphic modeling. Tectonics, 19(2), 225-240.

Reston, T. J., 2005, Polyphase faulting during the development of the west Galicia rifted margin, Earth and Planetary Science Letters, 237, 561-576.

Roberts, A. M., Yielding, G., Kusznir, N. J., Walker, I. M., and Dorn-Lopez, D., 1995, Quantitative-analysis of triassic extension in the northern Viking-Graben, Journal of the Geological Society, 152, 15-26.

Rogers, N. W., 2006. Basaltic magmatism and the geodynamics of the east african rift system. Geological Society of America Bulletin, 101(7), 885-903.

Rosendahl, B.L., 1987, Architecture of continental rifts with special reference to east Africa, Annual Reviews of Earth and Planetary Sciences, 15, 445-503.

Schlische, R. W., and Anders, M. H., 1996, Stratigraphic effects and tectonic implications of the growth of normal faults and extensional basins, In K. K. Beratan (Ed.), Reconstructing the history of Basin and Range extension using sedimentology and stratigraphy, Geological Society of America Special Paper 303, 183-203.

Scholz, C. H., Dawers, N. H., Yu, J.-Z., Anders, M. H. and Cowie, P. A., 1993, Fault growth and fault scaling laws: preliminary results, J. Geophys. Res. 98, 21,951-21,961.

Schöpfer, M. P., Childs, C., & Walsh, J. J., 2006, Localisation of normal faults in multilayer sequences, Journal of Structural Geology, 28, 816-833.

Schöpfer, M. P., Childs, C., Walsh, J. J., Manzocchi, T., & Koyi, H. A., 2007, Geometrical analysis of the refraction and segmentation of normal faults in periodically layered sequences, Journal of Structural Geology, 29, 318-335.

Sengör, A.M.C. and Burke, K., 1978. Relative timing of rifting and volcanism on Earth and its tectonic implications. Geophysical Research Letters, 5, 419–421.

Serra, S., and R. A. Nelson, 1989, Clay modelling of rift asymmetry and associated structures, Tectonophysics, 153, 307-312.

Shudofsky, G. N., Cloetingh, S., Stein, S., & Wortel, R., 1987. Unusually deep earthquakes in East Africa: Constraints on the thermo-mechanical structure of a continental rift system. Geophysical Research Letters.

Soliva, R., Schultz, R. A., and Benedicto, A. 2005, Three□dimensional displacement-length scaling and maximum dimension of normal faults in layered rocks, Geophysical Research Letters, 32, L16302.

Steel, R., and Ryseth, A., 1990, The Triassic - Early Jurassic succession in the northern North-Sea - Megasequence stratigraphy and intra-Triassic tectonics, Tectonic Events Responsible for Britains Oil and Gas Reserves, 55, 139-168.

Strecker, M. R., Blisniuk, P. M., and Eisbacher, G. H., 1990, Rotation of extension direction in the central Kenya Rift, Geology, 18, 299-302.

Taylor, S. K., Nicol, A., and Walsh, J.J., 2008, Displacement loss on growth faults due to sediment compaction, J. Struct. Geol., 30, 394-405.

Taylor, S., Bull, J.M., Lamarche, G., Barnes, P.M., 2004, Normal fualt growth and linkage in the Whakatane Graben, New Zealand, during the last 1.3 Myr, Journal of Geophysical Research, 109, B02408.

Ten Veen, J. H., & Kleinspehn, K. L., 2000, Quantifying the timing and sense of fault dip slip: new application of biostratigraphy and geohistory analysis, Geology, 28, 471-474.

Thomas, D. W., and Coward, M.P, 1995, Late Jurassic-Early Cretaceous inversion of the northern East Shetland Basin, northern North Sea, Geological Society, London, Special Publications, 88, 275-306.

Tomasso, M., Underhill, J. R., Hodgkinson, R. A., and Young, M. J., 2008, Structural styles and depositional architecture in the Triassic of the Ninian and Alwyn North fields: Implications for basin development and prospectivity in the Northern North Sea, Marine and Petroleum Geology, 25, 7, 588-605.

Trudgill, B., and Cartwright, J., 1994, Relay-ramp forms and normal-fault linkages, Canyonlands National Park, Utah, Geological Society of America Bulletin, 106, 1143-1157.

Turcotte, D.L., 1983. Driving mechanisms of mountain building. In: Mountain Building Processes (ed. by K.J. Hsu), Academic Press, Orlando, Florida, 141–146.

Walsh, J. J., and Watterson, J., 1988, Analysis of the relationship between displacements and dimensions of faults, Journal of Structural Geology, 10, 239-247.

Walsh, J. J., Bailey, W. R., Childs, C., Nicol, A., & Bonson, C. G., 2003, Formation of segmented normal faults: a 3-D perspective, Journal of Structural Geology, 25, 1251-1262.

Walsh, J. J., Nicol, A., & Childs, C., 2002. An alternative model for the growth of faults. Journal of Structural Geology, 24, 1669-1675.

Watterson, J., 1986. Fault dimensions, displacements and growth. Pure and Applied Geophysics 124, 365– 373.

Wernicke, B., 1985, Uniform-sense normal simple shear of the continental lithosphere, Canadian Journal of Earth Sciences, 22, 108-125.

Whipp, P., Jackson, C., Gawthorpe, R., Dreyer, T., Quinn, D., 2014. Normal fault array evolution above a reactivated rift fabric; a subsurface example from the northern Horda Platform, Norwegian North Sea. Basin Research 26, 523-549.

Withjack, M. O., and Jamison, W. R., 1986, Deformation produced by oblique rifting, Tectonophysics, 126, 2-4, 99-124.

Yirgu, G., Ebinger, C. J., & Maguire, P. K. H., 2006. The afar volcanic province within the east african rift system: introduction. Geological Society of London, 259(1), 1-6.

Young, M.J., Gawthorpe, R.L., Hardy S., 2001. Growth and linkage of a segmented normal fault zone; the Late Jurassic Murchison–Statfjord Fault, northern North Sea, Journal of Structural Geology, 23, 1933-1952.

Ziegler, P. A., and Cloetingh, S., 2004, Dynamic processes controlling evolution of rifted basins, Earth Sci. Rev., 64, 1-50.

Zoback, M. L., 1989. State of stress and modern deformation of the northern basin and range province. Journal of Geophysical Research Solid Earth, 94(B6), 7105–7128.

PAPER I

Influence of fault reactivation during multiphase rifting: the Oseberg area, Northern North Sea rift

Chao Deng[1], Haakon Fossen[2, 1], Robert L. Gawthorpe[1], Atle Rotevatn[1],

Christopher A-L. Jackson[3], Hamed FazliKhani[1]

[1] Department of Earth Science, University of Bergen, Allégaten 41, 5007 Bergen, Norway
[2] Museum of Natural History, University of Bergen, Allégaten 41, 5007 Bergen, Norway
[3] Basins Research Group (BRG), Department of Earth Science & Engineering, Imperial College, Prince Consort Road, London, SW7 2BP, UK

E-mail address: Chao.Deng@geo.uib.no, dengchao0926@gmail.com

Keywords: Multiphase rifting, Inter-rift fault activity, Structural inheritance, Fault interaction

Abstract

Multiphase rifts tend to produce fault populations that evolve by the formation of new faults and reactivation of earlier faults. The resulting fault patterns tend to be complex and difficult to decipher. In this work we use seismic reflection data to examine the evolution of a normal fault network in the Oseberg Fault Block in the northern North Sea Rift System – a rift system that experienced Permian – Early Triassic and Middle Jurassic – Early Cretaceous rifting and exhibits N-S, NW-SE and NE-SW oriented faults.

Both N-S- and NW-SE-striking faults were established during the Permian – Early Triassic rifting, as indicated by Triassic growth packages in their hanging walls. In contrast, the NE-SW-striking faults are younger, as they show no evidence of Permian – Early Triassic growth, and offset several N-S- and NW-SE-striking faults. Structural analysis show that a new population of NW-SE-striking faults formed in the Lower – Middle Jurassic (inter-rift period) together with reactivation of N-S-striking Permian – Early Triassic faults, indicating a NE-SW inter-rift extension direction.

During the Middle Jurassic – Early Cretaceous rifting, faults of all orientations (N-S, NW-SE and NE-SW) were active. However, faults initiated during the Middle Jurassic – Early Cretaceous rifting show mainly N-S orientation, indicating E-W extension

during this phase. These observations suggest a reorientation of the stress field from E-W during the Permian – Early Triassic rift phase to NE-SW during inter-rift fault growth and back to E-W during the Middle Jurassic – Early Cretaceous rift phase in the Oseberg area. Hence, the current study demonstrates that rift activity between established rift phases can locally develop faults with new orientations that add to the geometric and kinematic complexity of the final fault population.

1. Introduction

Many rift basins are known to have developed through multiphase rifting, such as the North Sea rift system (Badley et al., 1988; Færseth, 1996; Odinsen et al., 2000a; Whipp et al., 2014), the Gulf of Aden (Lepvrier et al., 2002), the East African Rift System (Korme et al., 2004) and the North West Shelf, Australia (Frankowicz and McClay, 2010). As for the northern North Sea rift system, two rift phases are recognized: the ?Permian – Early Triassic and the Middle Jurassic – Early Cretaceous rift phases (Badley et al., 1988; Bell et al., 2014; Færseth, 1996; Færseth et al., 1997; Steel and Ryseth, 1990; Yielding et al., 1992). The early consensus was that some of the faults initiated during the Permian – Early Triassic rifting were reactivated and played a significant role during the Middle Jurassic – Early Cretaceous rift phase, while others were not (Badley et al., 1988; Roberts et al., 1993, 1995; Steel and Ryseth, 1990; Yielding et al., 1992). A recent study showed that reactivated Permian – Early Triassic faults interacted with newly formed faults in various styles during the Middle Jurassic – Early Cretaceous rifting, forming non-collinear fault geometries (Duffy et al., 2015). However, fault evolution during the two rift phases is not clearly understood, and particularly not the way that Permian – Early Triassic faults reactivated and influenced fault growth during the second phase of rifting.

In this contribution we use 2D and 3D seismic reflection and borehole data to investigate the geometry and evolution of normal faults that evolved over the entire history of rifting in the Oseberg area in the northern North Sea. The Oseberg area is located at the boundary between the Permian – Early Triassic and Middle Jurassic – Early Cretaceous rift axis (Badley et al., 1984; Færseth et al., 1997; Færseth and Ravnas, 1998; Tomasso et al., 2008), making it possible to study the faults related to

both rift phases. The main goal is to understand the fault evolution and interaction between the two phases of rift-related faulting, and to explore what controls fault evolution in the Oseberg area and in multiphase rift basins in general.

2. Geological setting

The North Sea Rift System is built on originally overthickened Caledonian crust, thinned during post-collisional Devonian extension and erosion (Fossen, 2010). The Devonian, post-collisional extension resulted in the development of shear zones, such as those located onshore West Norway (Andersen & Jamtveit, 1990; Fossen, 1992; Vetti and Fossen, 2012) and probably also in the North Sea basement (Fossen et al., 2016). Hence, the Late Paleozoic-Mesozoic North Sea rift system developed on top of a basement containing both Caledonian and Devonian shear zones (Fig. 1A) (e.g. Bartholomew et al., 1993; Glennie, 1987; Smethurst, 2000; Stewart et al., 1992; Ziegler, 1990). The Permian-Early Triassic rifting lasted for 25-37 m.y. (e.g. Ter Voorde et al., 2000; Ziegler, 1990, 1992) and was followed by 70 m.y. of relative tectonic quiescence and post-rift thermal subsidence (e.g. Bartholomew et al., 1993; Glennie, 1987; Lepercq and Gaulier, 1996; Roberts et al., 1995; Ziegler, 1990). The Middle Jurassic – Early Cretaceous rift phase (e.g. Badley et al., 1988; Coward et al., 2003; Cowie et al., 2005; Roberts et al., 1995; Underhill and Partington, 1993) led to the superimposition of rift-related extension onto the thermally subsiding basin (e.g. Færseth,1996; Roberts et al., 1995).

Rift-related normal faults in the northern North Sea strike N-S, NE-SW and NW-SE, and relate to both phases of extension (Fig. 1) (Badley et al., 1984; Bell et al., 2014; Færseth and Ravnas, 1998; Odinsen et al., 2000b; Roberts et al., 1993; Steel and Ryseth, 1990). Permian – Early Triassic rifting is generally assumed to have occurred during E-W extension, as indicated by the predominantly N-S-orientation of major basin bounding and intra-basinal faults. An E-W extension direction is also supported by onshore kinematic analysis of Permo – Triassic dikes along the Norwegian rift shoulder (Fossen, 1998). Much of the Permian – Early Triassic extension was localized to the Horda Platform region (130-150 km wide), although rifting was important all across the Horda Platform – Viking Graben – Shetland Platform – West

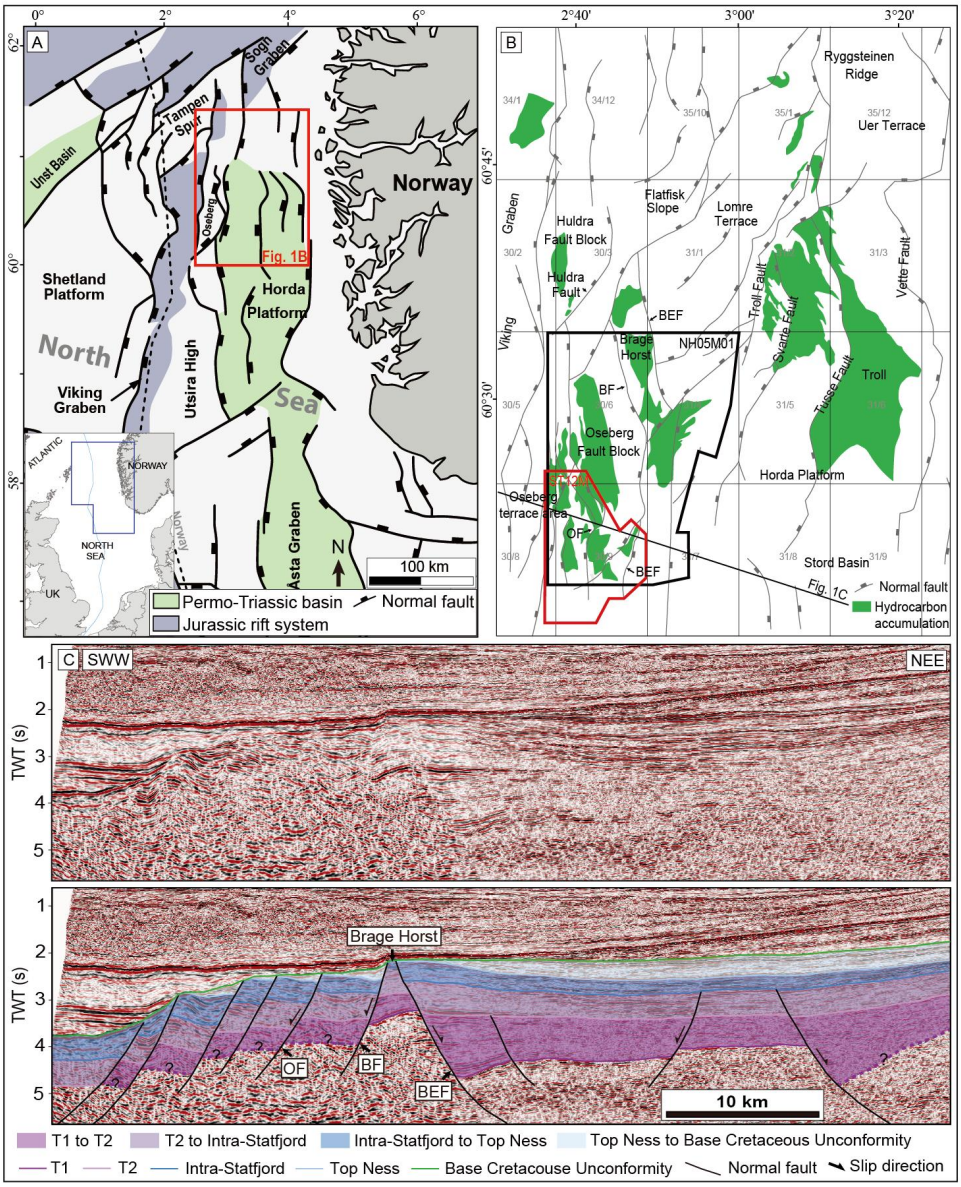

Fig. 1. (A) Simplified structural map of the northern North Sea rift, showing areas most affected by the two rift phases. After Færseth (1996). (B) Major structural elements and hydrocarbon accumulations (green) in the Oseberg and surrounding areas, according to Norwegian Petroleum Directorate (http://www.npd.no/en/). (C) 2D line across the Oseberg area and Horda Platform. OF-Oseberg Fault, BF-Brage Fault, BEF-Brage East Fault.

Shetland Basin area (Færseth, 1996; Odinsen et al., 2000b; Ter Voorde et al., 2000). In contrast, the Middle Jurassic – Early Cretaceous extension direction is more poorly constrained. Some authors suggest that it was coaxial with the Permian – Early Triassic rifting (Badley et al., 1988; Doré and Gage, 1987; Roberts et al., 1990) whereas others suggest WNW-ESE to NW-SE extension direction (Davies et al., 2001; Færseth, 1996; Færseth et al., 1997). The Middle Jurassic – Early Cretaceous extension is concentrated within the 25-40 km wide Viking Graben and the Sogn Graben (Fig. 1A) (Færseth, 1996; Odinsen et al., 2000b), while the Horda Platform itself underwent limited extension during this phase (Bell et al., 2014; Cowie et al., 2005; Færseth, 1996).

The study area is situated on the marginal part of the Horda Platform immediately east of the North Viking Graben, and comprises the Brage Horst, the Oseberg Fault Block, and the Oseberg terrace area (Fig 1B). The Brage Horst is bounded by the 80 km long E-dipping Brage East Fault to the east, and the 60 km long W-dipping Brage Fault to the west. The Oseberg Fault Block lies west of the Brage Horst and is bounded by the Brage and Oseberg faults in the east and west, respectively. Further to the west of the Oseberg Fault Block is the Oseberg terrace area.

The oldest stratigraphic unit drilled in the study area is of upper Triassic age (Well 31/4-2 in Fig. 2). The Triassic Hegre Group comprises mainly continental sandstones and mudstones and is interpreted to be mainly the lower part of the inter-rift unit (Lervik, 2006; Steel and Ryseth, 1990)(Fig. 2). In the Early to Middle Jurassic, a fluvio-deltaic to shallow marine succession was deposited in the upper part of the inter-rift package that includes the Statfjord, Dunlin and Brent Groups (Færseth and Ravnas, 1998; Helland-Hansen et al., 1992; Steel, 1993). The Middle Jurassic – Early Cretaceous syn-rift strata are generally made up of the marine Viking Group, including shallow marine clastic sequences of the Heather Formation (Dreyer et al., 2005; Færseth and Ravnas, 1998) and deep marine mudstones of the Draupne Formation. However, in some places the initiation of Middle Jurassic – Early Cretaceous rifting coincides with the deposition of the upper part of the Brent Group (uppermost of Ness and Tarbert formations) (Helland-Hansen et al., 1992; Yielding et al., 1992). The

Viking Group is capped by the Base Cretaceous Unconformity in this area which, for the most part, marks the end of the Middle Jurassic – Early Cretaceous rift Phase (Kyrkjebø et al., 2004). The Base Cretaceous Unconformity is overlain by a post-rift succession that is composed of deep-water clastics and carbonates of the Cromer Knoll and Shetland groups, and mud-dominated Cenozoic strata (Fig. 2).

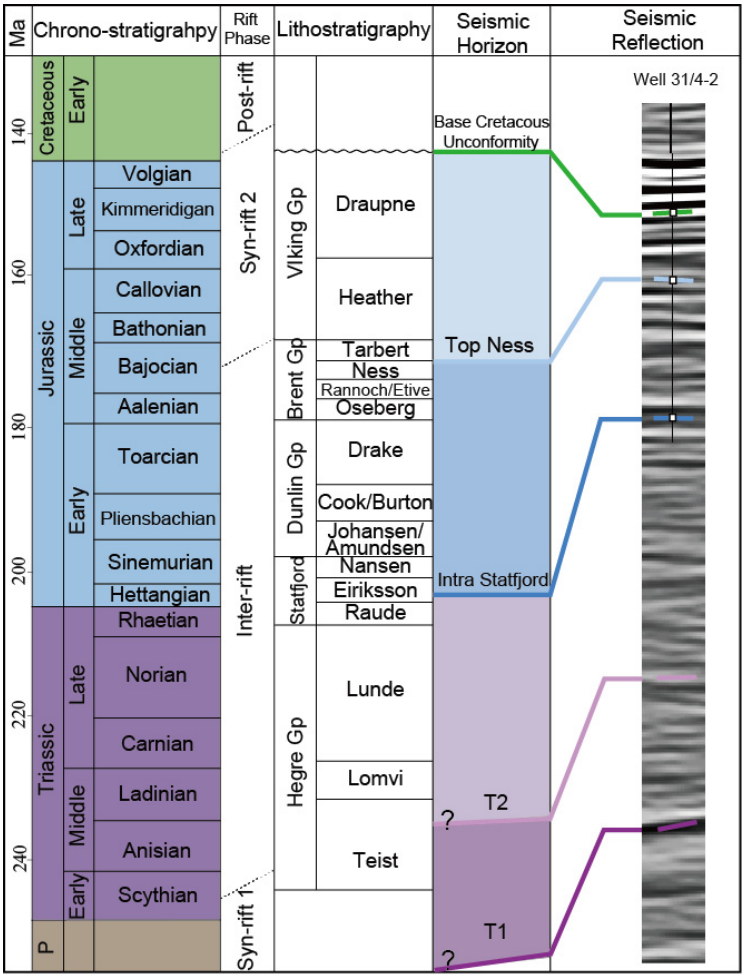

Fig. 2. Stratigraphic column in northern North Sea, after Bell et al. (2014) and Færseth (1996). The stratigraphic ages of T2 and T1 are uncertain owing to the lack of stratigraphic data from well.

3. Data and methods

This study is based on 2D and 3D seismic reflection data. Two 3D seismic cubes, ST12M and NH05M01 in Fig. 1B, covering the Oseberg Fault Block and Brage Horst, are used for the study. The seismic cubes cover ~450 km^2 and ~1500 km^2, respectively, with a line spacing of 12.5 m. The cube ST12M images down to 5.5 s TWT, while the cube NH05M01 displays data down to 3.5 s TWT. The seismic is displayed in normal polarity (SEG Convention), whereby a downward increase in acoustic impedance is indicated by a peak (bright reflection) and a decrease in acoustic impedance is represented by a trough (black reflection) (Fig. 2). The 2D seismic line, striking NNW-SSE, crosses the south of the study area (Fig. 1B). In addition, forty-six wells are tied to the seismic data by means of synthetic seismograms, covering most parts of the study area (Fig. 3). The majority of the wells penetrate the Brent Group, but only a few (e.g. 31/4-2 in Fig. 2) of them reach the top Triassic.

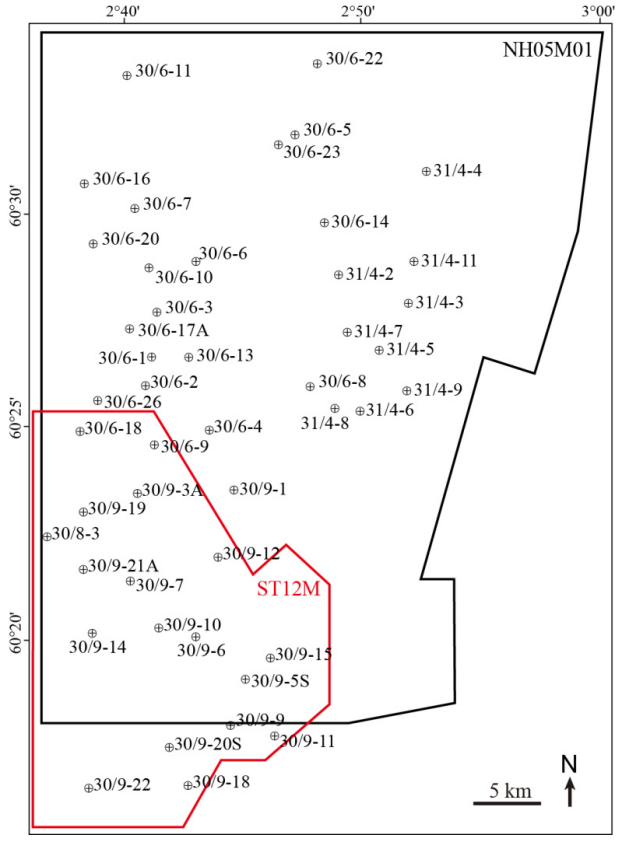

Fig. 3. Well location map in the two seismic cubes of the study area. See Fig. 1B for location.

Five seismic horizons have been interpreted: Base Cretaceous Unconformity, Top Ness, Intra-Statfjord, T2 and T1 (Fig. 2). T2 and T1 are pre-late Triassic horizons. T1 is a strong reflector deeper than 3.5 ms TWT in the study area, and is only mapped in the cube ST12M owing to poor or lack of data in other areas (Fig. 4A). Reflection T2 is strong in the east but relatively weak to the west of cube ST12M, in which case its interpretation is guided by over- or underlying reflections. Intra-Statfjord, Top Ness and Base Cretaceous Unconformity are strong and continuous reflections and mapped across the two seismic cubes (Fig. 4C-D). The horizons were interpreted at an increment of every sixteen lines (~200 m).

Based on the seismic interpretation, we use four methods to analyze fault geometry and evolution: (i) throw-length (T-x) plots, which display fault throw for a particular horizon against the distance along the fault, and are used to study the growth and linkage of fault systems (e.g. Baudon and Cartwright, 2008a; 2008b; Cartwright et al., 1995; Dawers and Anders, 1995; Gupta and Scholz, 2000; Peacock and Sanderson, 1991; Young et al., 2001); (ii) throw-depth (T-z) profiles, which record fault throw for all interpreted horizons and yield information that can be used to interpret the vertical propagation history of faults (Baudon and Cartwright, 2008a, 2008b, 2008c; Cartwright et al., 1998; Hongxing and Anderson, 2007); (iii) strike projection of fault throw, which allows the 3D fault growth history to be investigated (Walsh and Watterson, 1991); and (iv) time-thickness maps, created by calculating the difference in TWT between two horizons to tracks spatial variations in subsidence, are used to determine fault activity during those time intervals.

Fault throw, as measured on seismic sections that are oriented perpendicular to local fault strike, is the vertical distance between hanging wall and footwall cut-offs. Ductile displacement represented by fault drag was accounted for by extrapolating the reflectors to the fault along the trend of the horizon outside of the drag zone (Long and Imber, 2010; Whipp et al., 2014). Where sediment is partly or fully eroded in the footwall, faults and horizons were projected using local dip and stratigraphic thickness data.

4. Structural style of the Oseberg area

The 2D transect in Fig. 1C shows that faults are mostly E-dipping east of the Brage Horst, bounding the Permian – Early Triassic growth packages (T1 – T2 in Fig. 1C). In contrast, faults are mostly W-dipping to the west of the Brage Horst, bounding the Middle Jurassic – Early Cretaceous growth packages (Top Ness – Base Cretaceous Unconformity in Fig 1C). In map view, faults can be divided into two groups: (i) major faults that are >20 km in length and show >200 ms TWT of maximum throw of the Top Ness horizon; and (ii) minor faults that are <15 km long and show <200 ms TWT of maximum throw at this level.

4.1. Major faults

Major faults are curved in map view, including the Brage East Fault, Brage Fault and Oseberg Fault, in addition to some faults to the west of the Oseberg Fault (Fig. 4).

4.1.1. Brage East Fault

The E-dipping Brage East Fault (BEF) contains three separated segments at the Intra-Statfjord and Top Ness horizons: BEF1 (~5 km long) striking NNW-SSE, BEF2 (~20 km long) striking NNW-SSE to N-S and, BEF3 (~15 km long) striking NNE-SSW to N-S toward the south (Fig. 4). Between the three segments develop the W-dipping Brage Fault and F12, at which the segments of the Brage East Fault terminate. However, the Brage East Fault cuts through the T1 to T2 package (Fig. 5), indicating that the Brage East Fault is laterally continuous in the T1 to T2 package. In the vertical direction, the Brage East Fault tips-out at the Base Cretaceous Unconformity and extends downward into the basement (Fig. 5). In the hanging wall of the Brage East Fault, the T1 to T2 package is wedge-shaped and W-expanding (Fig. 1C), whereas the T2 to Base Cretaceous Unconformity package is tabular to sub-tabular (Fig. 5).

Fig. 4. TWT structure map of four key horizons. (A) T1 is a syn-rift 1 horizon. The white area which is not interpreted is owing to the poor seismic data. (B) T2, (C) Intra-Statfjord and (D) Top Ness, representing three horizons within the inter-rift strata, showing map view fault geometries. OF-Oseberg Fault, BF-Brage Fault, BEF-Brage East Fault.

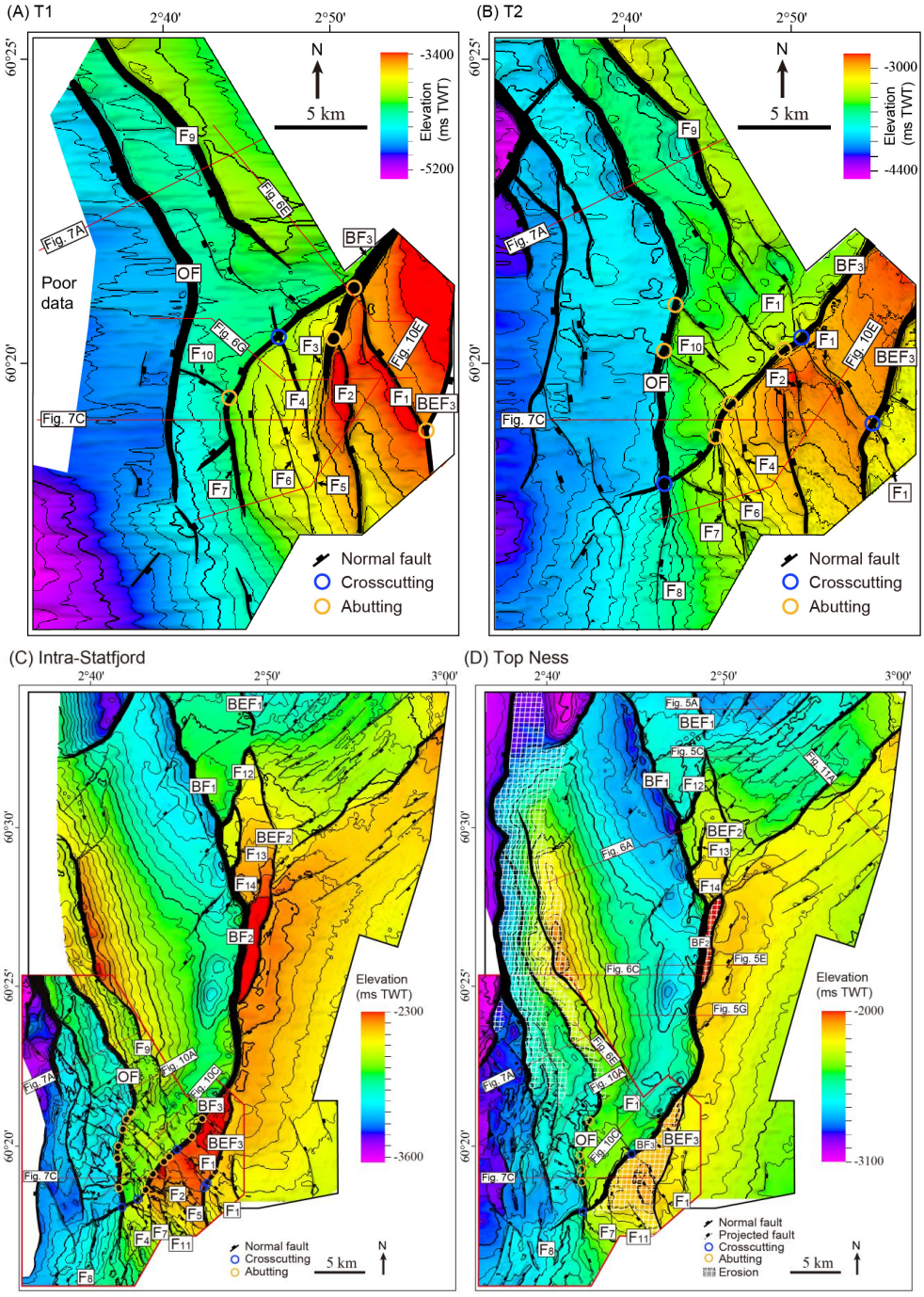
(A) T1
(B) T2
(C) Intra-Statfjord
(D) Top Ness
2°40'
2°50'
3°00'
60°25'
60°20'
60°30'
N
5 km
Elevation (ms TWT)
-3400
-5200
-3000
-4400
-2300
-3600
-2000
-3100
Poor data
OF
BF1
BF2
BF3
BEF1
BEF2
BEF3
F1
F2
F3
F4
F5
F6
F7
F8
F9
F10
F11
F12
F13
F14
Fig. 5A
Fig. 5C
Fig. 5E
Fig. 5G
Fig. 6A
Fig. 6C
Fig. 6E
Fig. 6G
Fig. 7A
Fig. 7C
Fig. 10A
Fig. 10C
Fig. 10E
Fig. 11A
Normal fault
Projected fault
Crosscutting
Abutting
Erosion

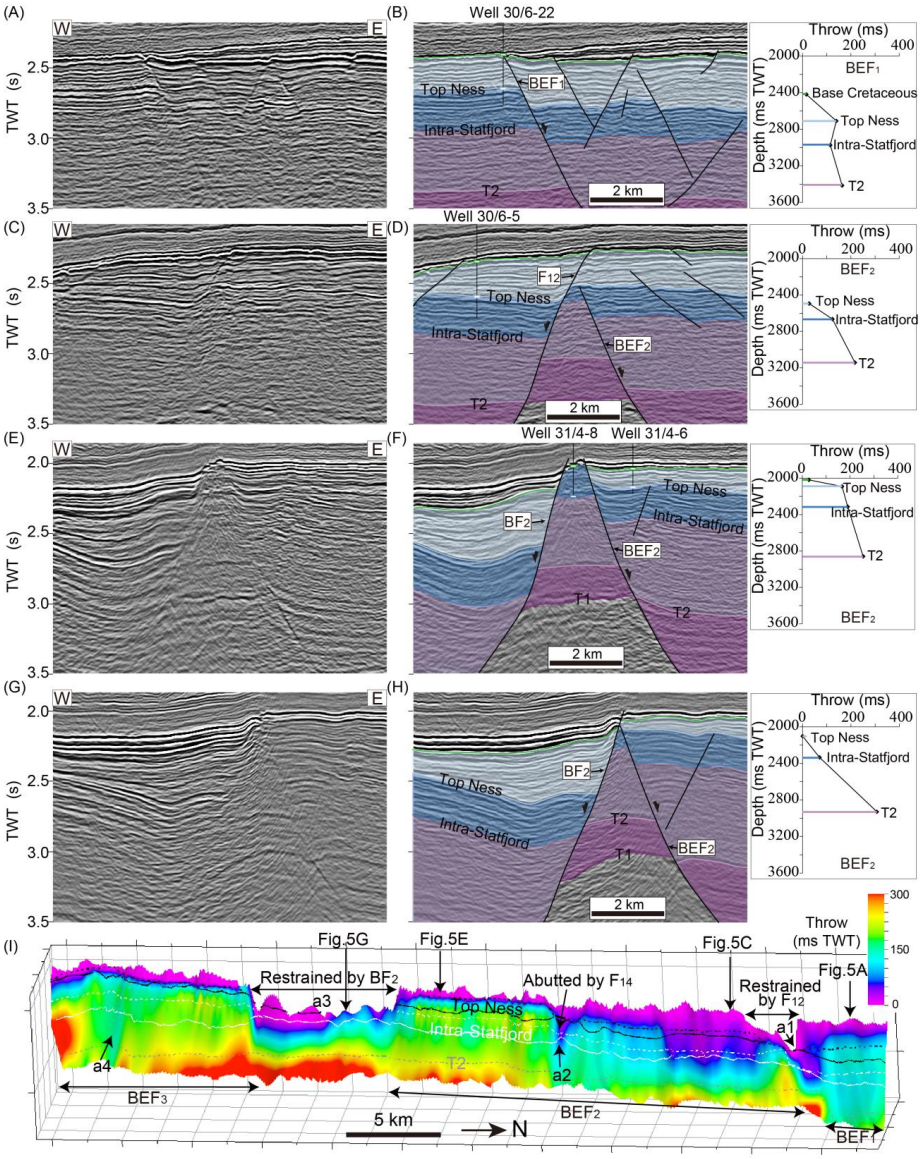

Fig. 5. Geometry of the Brage East Fault. (A)-(H) are four uninterpreted and interpreted cross-sections sub-perpendicular to the Brage East Fault. See Figs. 4 and 5I for locations. The colors used for the key horizons and the interval between them are consistent with those used in Fig. 2. T-z plots of the Brage East Fault are shown in the right column. (I) Strike projection on the Brage East Fault, as viewed from the hanging-wall side of the fault. Solid lines on the fault plane are the hanging-wall cut-off lines. Dashed lines are footwall cut-off lines. 'a1'-'a4' represent throw minima or gaps.

T-z profiles and strike projection of the Brage East Fault display a downward increase in fault throw from the Base Cretaceous Unconformity to T2 (Fig. 5). Based on the present 3D seismic data, its throw is ~300 ms TWT (~500 m) at the deepest mapped level (T2). The throw of the Brage East Fault at the T1 level is over 1200 ms TWT (~2000 m) according to the 2D transect (Fig. 1C). Throw minima occur at locations 'a1'-'a4' on the strike projection (Fig. 5I). Specifically, the upper tip of the Brage East Fault shows a non-elliptical shape, with gaps at 'a1' and 'a3' (Fig. 5I), where it terminates in the immediate footwall of the F12 and Brage Fault (Fig. 5I). The 'a2' gap is related to the intersection with the F14, whereas 'a4' corresponds to the change in strike from N-S to NNE-SSW toward the north (Fig. 5I).

4.1.2. Brage Fault

The whole Brage Fault (BF) is captured at the Intra-Stafjord and Top Ness horizons by the seismic cube NH05M01, displaying strike variations from NNW-SSE to N-S and then to NE-SW southward (Fig. 4C-D). For simplicity, the Brage Fault comprises three differently-striking segments: NNW-SSE-striking BF1 (~20 km), N-S-striking BF2 (~15 km) and NE-SW-striking BF3 (~20km). In cross-section, the upper tip of the Brage Fault extends upward into the Lower Cretaceous succession, and the NE-SW-striking segment (BF3) is basement rooted (Fig. 6). Clearly, the T1 to Top Ness package is tabular to sub-tabular, whereas the Top Ness to Base Cretaceous Unconformity package is E-expanding in the hanging wall of the Brage Fault (Fig. 6).

The segments BF1 and BF2 show a general increase in fault throw with depth (Fig. 6). Only the northern part of segment BF3 shows a slight decrease in fault throw at the T2 level (Fig. 6 I). In contrast, the southern part of the segment BF3 has a quick increase in fault throw from the Base Cretaceous Unconformity to Intra-Statfjord horizon and a slow decrease from Intra-Statfjord to T1 horizon (Fig. 6). Strike projection illustrates that the overall throw maximum of the Brage Fault is located at the central segment BF2 (~800 ms TWT or ~1200 m), from where the throw decreases radially (Fig. 6G). Local sharp changes in fault throw occur at locations 'b1'-'b3' on the segment BF1, related to the intersection with faults F12-F14 (Fig. 4D).

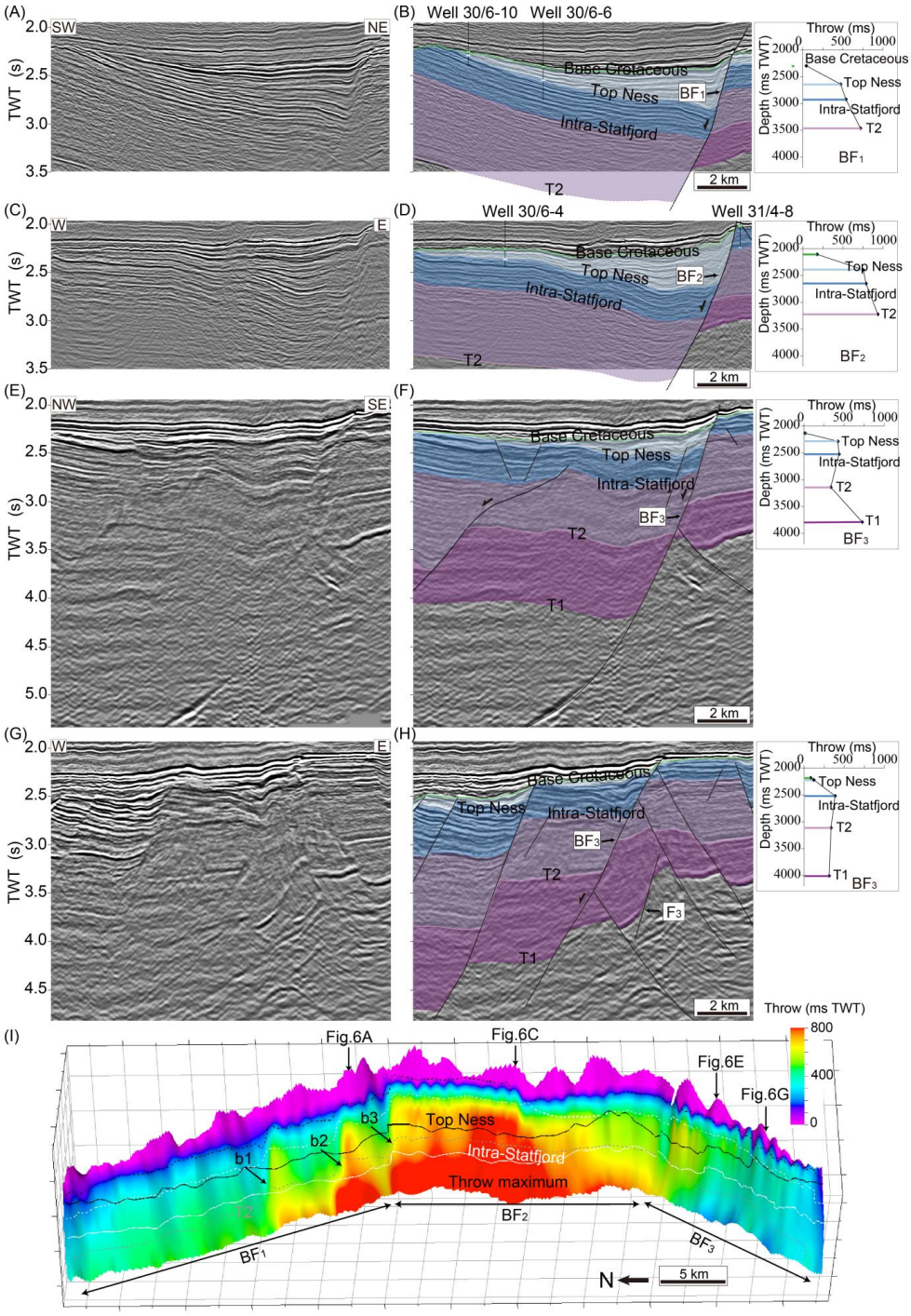
(A)
SW
NE
TWT (s)
2.0
2.5
3.0
3.5
(B) Well 30/6-10 Well 30/6-6
Base Cretaceous
Top Ness
BF1
Intra-Statfjord
T2
2 km
Throw (ms)
0 500 1000
Depth (ms TWT)
2000
2500
3000
3500
4000
Base Cretaceous
Top Ness
Intra-Statfjord
T2
BF1
(C)
W
E
TWT (s)
2.0
2.5
3.0
3.5
(D) Well 30/6-4 Well 31/4-8
Base Cretaceous
Top Ness
BF2
Intra-Statfjord
T2
2 km
Throw (ms)
0 500 1000
Depth (ms TWT)
2000
2500
3000
3500
4000
Top Ness
Intra-Statfjord
T2
BF2
(E)
NW
SE
TWT (s)
2.0
2.5
3.0
3.5
4.0
4.5
5.0
(F)
Base Cretaceous
Top Ness
Intra-Statfjord
BF3
T2
T1
2 km
Throw (ms)
0 500 1000
Depth (ms TWT)
2000
2500
3000
3500
4000
Top Ness
Intra-Statfjord
T2
T1
BF3
(G)
W
E
TWT (s)
2.0
2.5
3.0
3.5
4.0
4.5
(H)
Base Cretaceous
Top Ness
Intra-Statfjord
BF3
T2
F3
T1
2 km
Throw (ms)
0 500 1000
Depth (ms TWT)
2000
2500
3000
3500
4000
Top Ness
Intra-Statfjord
T2
T1
BF3
(I)
Fig.6A
Fig.6C
Fig.6E
Fig.6G
Throw (ms TWT)
800
400
0
b1
b2
b3
Top Ness
Intra-Statfjord
Throw maximum
T2
BF1
BF2
BF3
N
5 km

Fig. 6. Geometry of the Brage Fault. (A)-(H) are four uninterpreted and interpreted cross-sections sub-perpendicular to the fault local strike, across the three segments of the Brage Fault. See Figs. 4 and 6I for location of the cross-sections. The colors used for the key horizons and the intervals between them are consistent with those used in Fig. 2. T-z plots of the Brage Fault are put on the right of the interpretation. (G) Strike projection on the Brage Fault, as viewed from the hanging wall side of the fault. Solid lines on the fault plane are hanging wall cut-offs. Dashed lines are footwall cut-offs. 'b1'-'b3' show three locations of throw jumps on the fault plane.

4.1.3. Oseberg Fault

The W(SW)-dipping Oseberg Fault (OF) is ~35 km long, making a bend as it turns from NNW-SSE- to N-S-striking towards the south (Fig. 4D). Vertically, the upper tip of the Oseberg Fault is located either at or above the Base Cretaceous Unconformity, and the fault extends downwards into the basement (Fig. 7). In the hanging wall of the Oseberg Fault, the Top Ness to Base Cretaceous Unconformity package is E-expanding where not eroded, whereas the T1 to Top Ness package is tabular to sub-tabular (Fig. 7).

Strike projection and T-x plots of the portion of Oseberg Fault in the seismic cube ST12M shows throw minima at locations 'c1' and 'c2' (Fig. 7E, 8B). In addition, the throw of the Oseberg Fault drops abruptly (~100 ms TWT or ~150 m) south of the intersection with the NE-SW-striking segment of the Brage Fault ('c3' in Fig. 8B). Vertically, the NNW-SSE-striking segment of the Oseberg Fault increases in throw from the Top Ness to Intra-Statfjord, and increases again from T2 to T1 (Fig. 7E), obtaining a throw value of ~500 ms TWT (~750 m) at the T1 horizon (Fig. 7E). In contrast, throw maximum of the N-S-striking segment is best defined at the T2 horizon and equals ~400 ms TWT (~600 m), from where throw decreases upward and downward (Fig. 7E). In addition, throw of the horizons from Top Ness to T1 displays a rough trend of increase with depth on the NNW-SSE-striking segment of the Oseberg Fault (Fig. 9A). Back-stripping of the T-x plots shows that the fault has a maximum throw difference of ~120 ms TWT (~180 m) between horizons T1 and T2, ~300 ms

TWT (~450 m) between horizons T2 and Top Ness, and again ~300 ms TWT (~450 m) between Top Ness and the Base Cretaceous Unconformity (Fig. 9B-D).

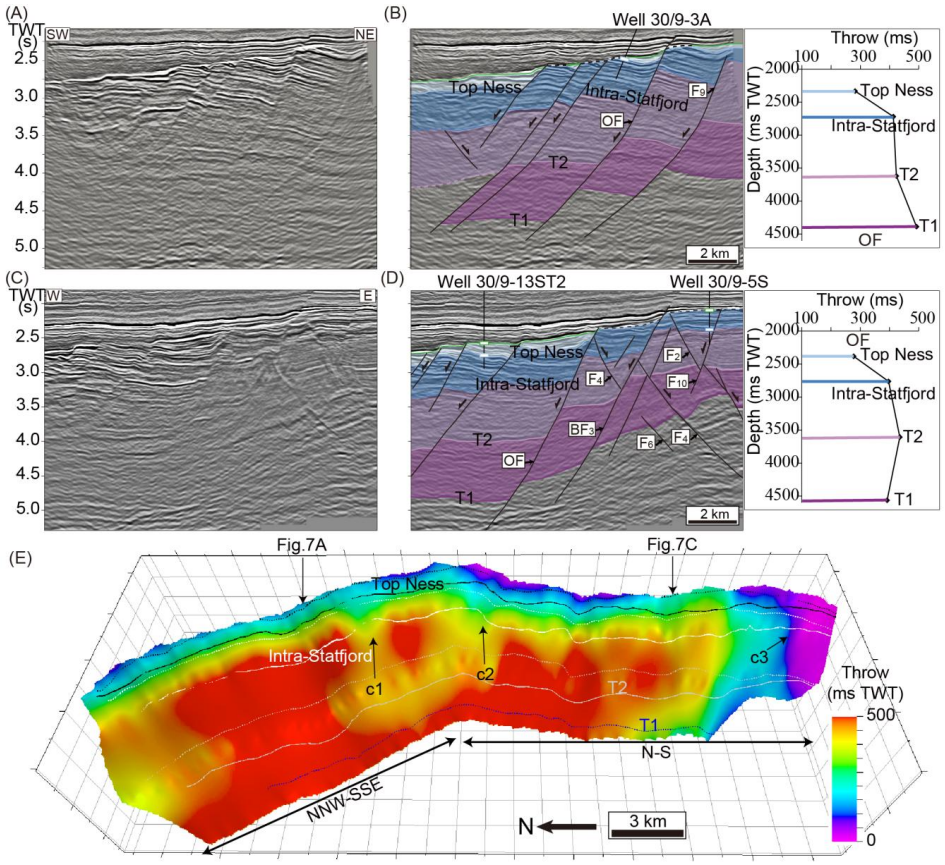

Fig. 7. Geometry of the Oseberg Fault. (A)-(D) are two uninterpreted and interpreted cross-sections sub-perpendicular to the local strike across the three segments of the Oseberg Fault. See Figs. 4 and 7E for location. The colors used for the key horizons and the intervals between them are consistent with those used in Fig. 2. T-z plots of the Brage Fault are shown in the right column. (E) Strike projection on the Oseberg Fault, as viewed from the hanging wall side. Solid lines on the fault plane are the cut-offs in the hanging wall. Dashed lines are footwall cut-offs lines. 'c1' and 'c2' show locations of throw minima. 'c3' represents the point of intersection with the Brage Fault.

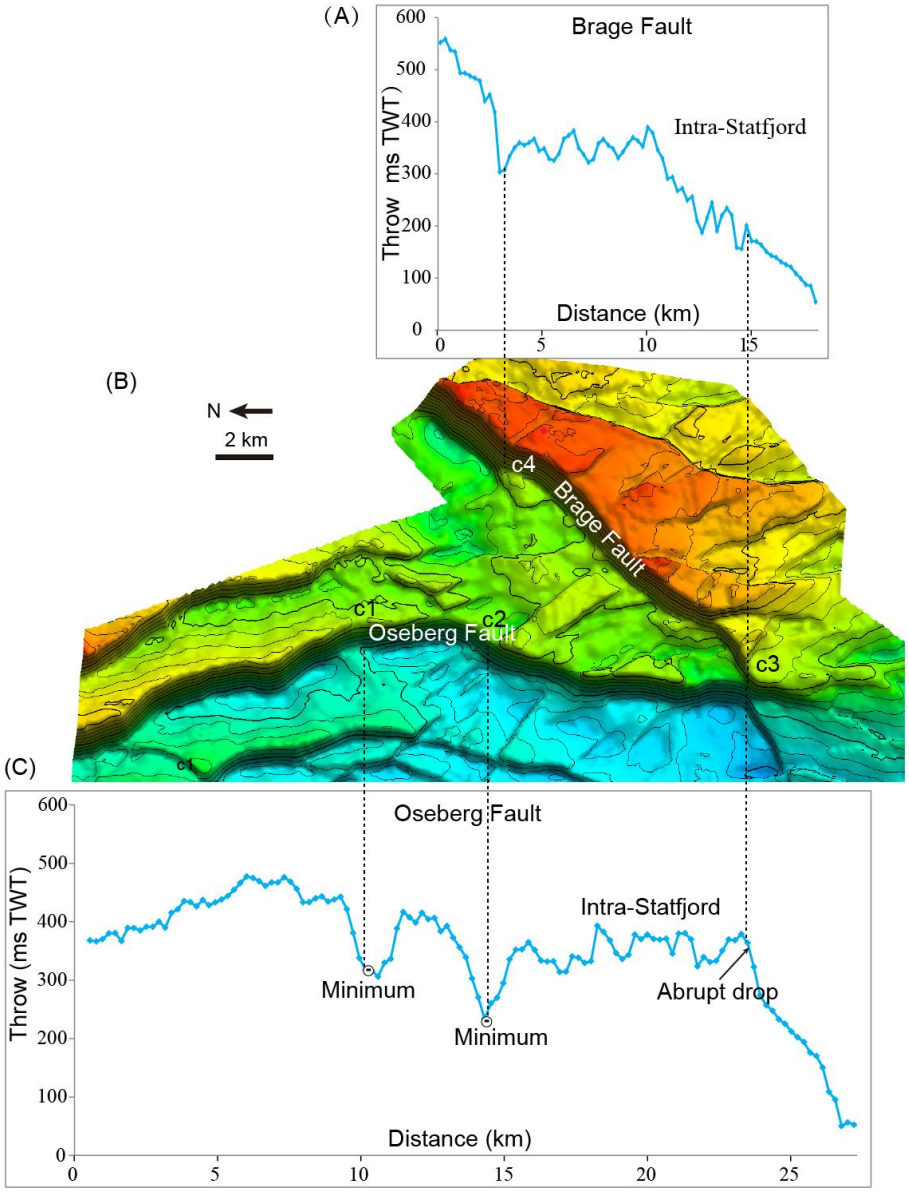

Fig. 8. T-x plots of the Oseberg Fault and the NW-SE-striking segment of the Brage Fault (BF_3) showing along-strike fault throw at the Intra-Statfjord horizon. (A) T-x plots of the Brage Fault, (B) Surface map showing the structure at the Intra-Statfjord horizon, (C) T-x plots of the Oseberg Fault. 'c1'-'c4' the location of intersection or orientation change, illustrates the corresponding position on the fault heave with T-x plots.

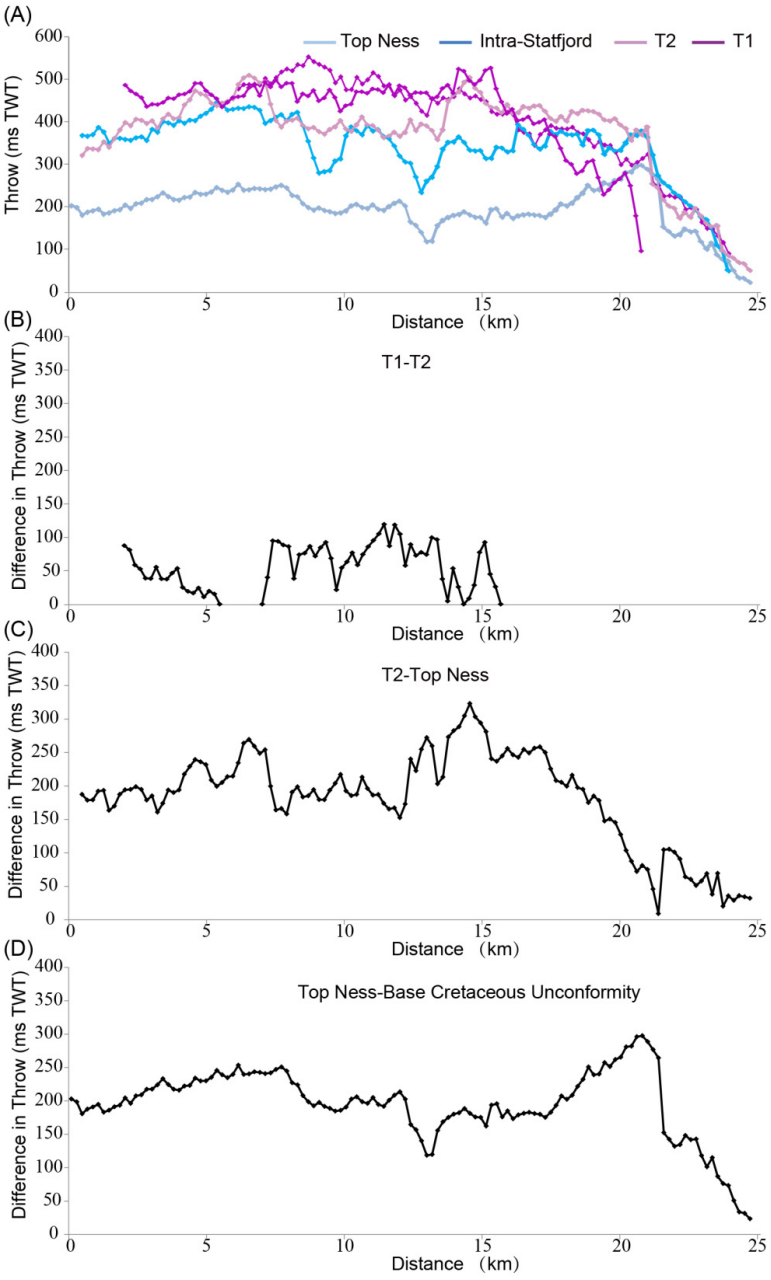

Fig. 9. (A) T-x plots of the Oseberg Fault at four horizons, show variation of fault throw along-strike and with depth. (B) The throw difference from T1 to T2 horizons. (C) The throw difference from T2 to Top Ness horizons. (D) The throw difference from Top Ness to Base Cretaceous.

4.2. Minor faults

Minor faults mainly occur in the southwest and northeast parts of the study area (Fig. 4C-D). In the southwest, minor faults are dominantly NW-SE-striking, with a few of them N-S-striking; in the northeast, they are NE-SW-striking (Fig. 4C-D).

The NW-SE-striking minor faults tip out upward in the Intra-Statfjord to Top Ness or Top Ness to Base Cretaceous Unconformity packages (Fig. 10). Growth packages are observed for the lower part of the Intra-Statfjord to Top Ness package across the NW-SE-striking minor faults in the hanging wall of the Oseberg Fault (Fig. 10B). In some cases, it is uncertain at what level the upper tips of minor faults reach, owing to the sub-Top Ness erosion (e.g. F2, F7, F10 and F11 in Fig. 10F), but some of them, such as F4, terminate below the Top Ness level (Fig. 10D). For the lower tip, some (e.g. F1-F2 in Fig. 10) are basement-rooted and bound a W-expanding T1-T2 package in the hanging wall; others (e.g. those in the hanging wall of F1 in Fig. 10B) tip out in the T1-T2 package, associated with an antithetic fault. In some cases a minor fault, such as F2, F3 or F4, is offset by the Brage Fault or another minor fault (Fig. 7D, 10D). More often, E-dipping minor faults are offset by W-dipping faults.

The NE-SW-striking minor faults generally extend upward into the Lower Cretaceous succession, and downward into the T2 to Intra-Statfjord package, with a few extending into the upper part of the T1 to T2 package (Fig. 11). Different from the NW-SE-striking minor faults, there is no obvious evidence of basement involvement for the NE-SW-striking minor faults. In addition, the Top Ness to Base Cretaceous Unconformity interval displays subtle wedge-shaped packages in the hanging wall of some NE-SW-striking minor faults, whereas the T2 to Top Ness package is roughly tabular (Fig. 11). Hence, most or all of NE-SW-striking minor faults initiated in the sedimentary rift fill.

4.3. Fault growth and interaction

The general increase in fault throw with depth and hanging wall growth packages of the T1-T2 and Top Ness-Base Cretaceous Unconformity intervals indicate that the Brage East Fault formed during the Permian – Early Triassic rift phase and reactivated

during the Middle Jurassic – Early Cretaceous rift phase. The gaps at locations ‘a1’ and ‘a3’ imply that the upper tip of the Brage East Fault is restrained at the intersection with the oppositely dipping F12 and Brage Fault (Fig. 5I). Therefore, the upward growth of the reactivated Brage East Fault was restrained where intersecting oppositely dipping faults. In this case, the upper tip of the restrained fault (BEF) exhibits an irregular geometry in three dimensions. In map view, the restrained fault shows some separated segments at the upper level that join into a single deep root at the bottom.

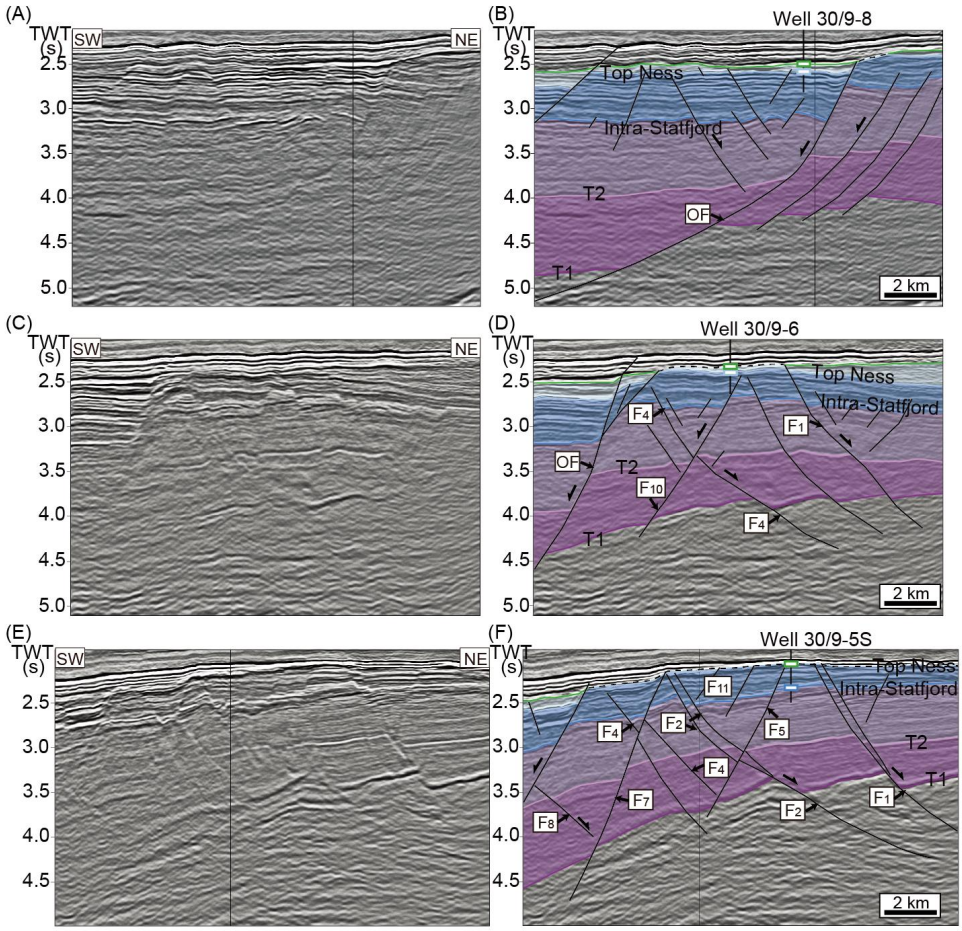

Fig. 10. Three cross-sections sub-perpendicular to the NW-SE-striking minor faults. The colors used for the key horizons and the interval between them are consistent with those used in Fig. 2. See Fig. 4 for location.

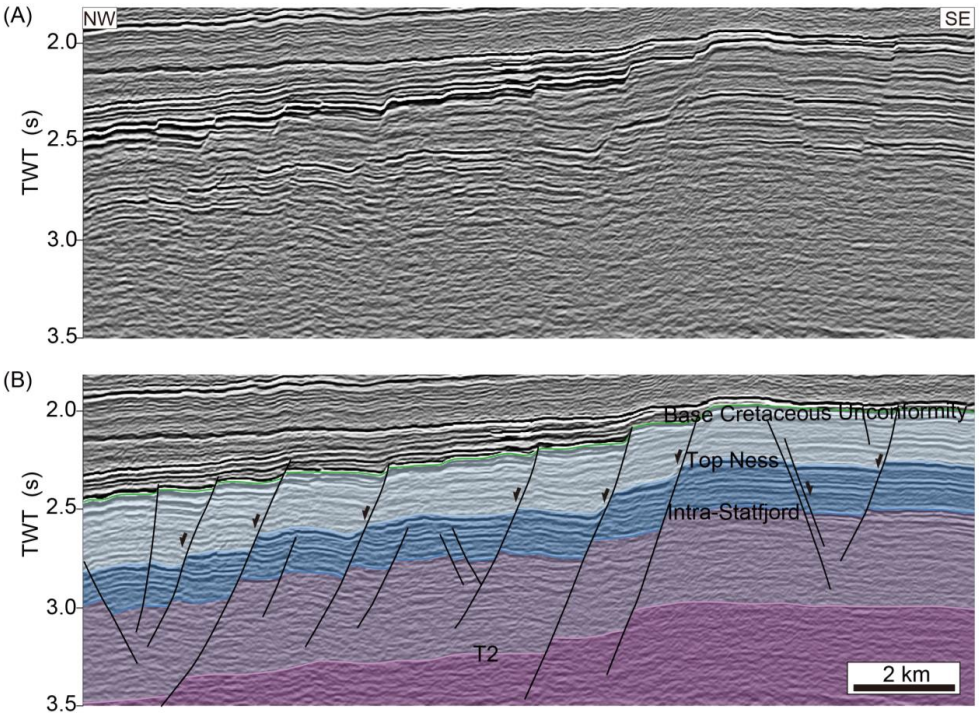

Fig. 11. Cross-section perpendicular to the trend of the NE-SW-striking minor faults. The colors used for the key horizons and the interval between them are consistent with those used in Fig. 2. See Fig. 4 for location.

The general downward increase in fault throw from the Base Cretaceous Unconformity to T2 of the NNW-SSE-, N-S- and northern part of the NE-SW-striking segment of the Brage Fault (Fig. 6) indicates that all of the segments originated from the Permian – Early Triassic rift phase, similar to the Brage East Fault. In contrast, the southern part of the NE-SW-striking segment of the Brage Fault (BF3) started to grow during the Middle Jurassic – Early Cretaceous rift phase. This is based on the Top Ness-Base Cretaceous Unconformity wedge-shaped growth package and downward decreasing fault throw from the Intra-Statfjord to T1 horizons (segment BF3 in Fig. 6I). The radial decrease in fault throw from the central N-S-striking segment probably suggests that the Brage Fault initiated at the N-S-striking segment, and then its northern tip propagated in the NNW-direction, while the southern tip propagated in the SW-direction. Another possibility is that the NNW-SSE-, N-S- and NE-SW-striking

segments nucleate at different locations, while the N-S-striking segment played a dominant role during the growth, grasping most of the strain and overprinting the initial throw maximum on the NNW-SSE- and NE-SW-striking segments after linkage.

The Oseberg Fault consisted of three segments separated by ‘c1’ and ‘c2’. This is indicated by: (i) the bend in the Oseberg Fault trace in map view; and (ii) the well-defined throw minima at ‘c1’ and ‘c2’ (Fig. 8C). The continuous increase in throw with depth illustrates that the Oseberg Fault has been a long-lived fault from its initiation during the Permian-Early Triassic rift phase, followed by a period of growth during the Middle Triassic-Middle Jurassic, with renewed growth during the Middle Jurassic-Early Cretaceous rift phase. In addition, throw difference from the T2 to Top Ness horizon is similar to that from the Top Ness to Base Cretaceous Unconformity horizon, meaning that fault activity during the Middle Triassic-Middle Jurassic is comparable to that of the Middle Jurassic-Early Cretaceous rift phase. Furthermore, the abrupt drop in throw of the Oseberg Fault at the intersection with the NE-SW-striking segment of the Brage Fault implies that the latter fault crosscut and displaced the already established and probably inactive Oseberg Fault during the Middle Jurassic – Early Cretaceous rift phase.

5. Fault evolution

Having established the structural style of the Oseberg area, now we investigate the overall evolution of the fault network. To accomplish this, cross-sectional geometry, throw measurement and time-thickness map are integrated.

5.1. T1 to T2 interval

Although the precise age of the T1-T2 package is unknown due to lack of borehole data, we assume, based on thickness changes and regional knowledge (e.g. Bell et al., 2015; Færseth, 1996; Steel and Ryseth, 1990) that it incorporates most or all of the syn-rift 1 package and the lower part of the inter-rift succession. Thickness increases occur across the minor faults F1 to F3, Brage East Fault (BEF3), the northern part of

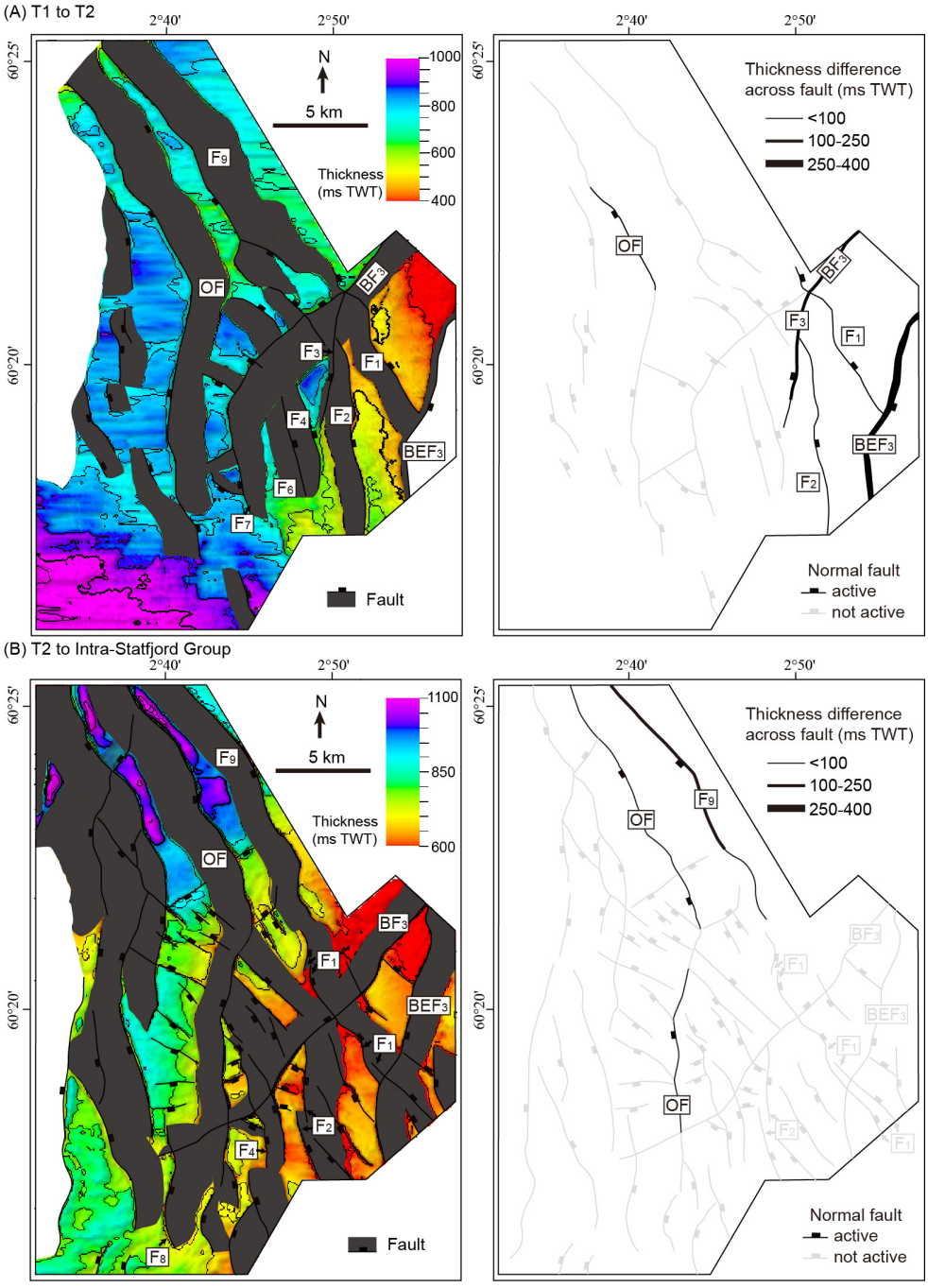
(A) T1 to T2
2°40'
2°50'
60°25'
60°20'
N
5 km
Thickness
(ms TWT)
1000
800
600
400
F9
OF
BF3
F3
F1
F4
F2
BEF3
F6
F7
Fault
Thickness difference
across fault (ms TWT)
<100
100-250
250-400
Normal fault
active
not active
(B) T2 to Intra-Statfjord Group
1100
850
600
F8

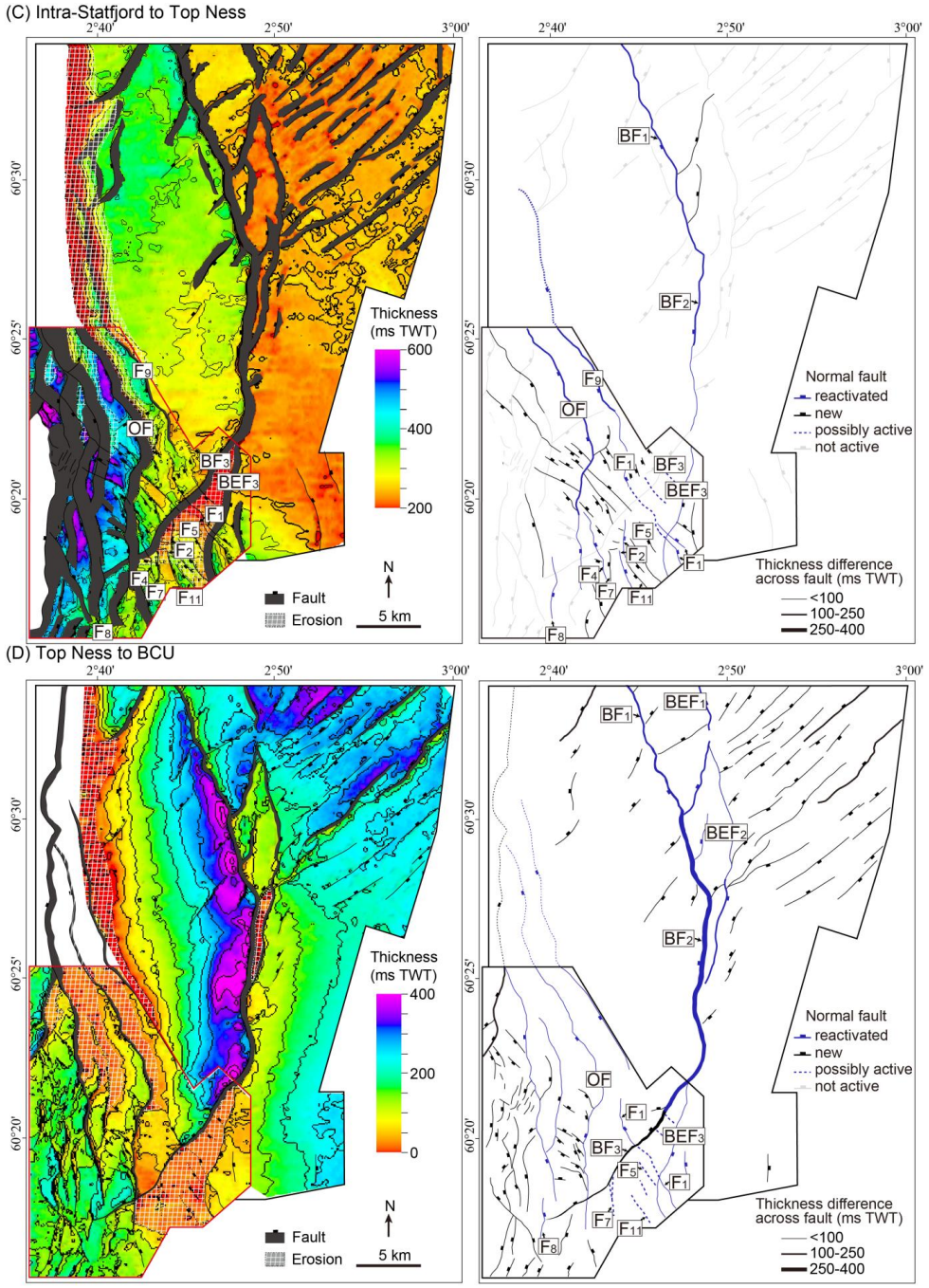

Fig. 12. Isochore maps of different time intervals showing the fault activity for each depositional period. (A) T1 to T2. (B) T2 to Intra-Statfjord. (C) Intra-Statfjord to Top Ness.

(D) Top Ness to BCU, erosion of the upper part of Brent Group in the footwall crest is covered in black. The dashed lines on Brage Horst show the location of possible active faults that were eroded in the late Jurassic.

the NE-SW-striking segment of the Brage Fault (BF3) and the NNW-SSE-striking segment of the Oseberg Fault (OF) (Figs. 7 and 12A). Subtle wedge-shaped growth packages for this unit are observed in the hanging wall of F1 and F2 (Fig. 6H, 10), and are particular notable for the Brage East Fault (BEF) (Fig. 1C).

We interpret the minor faults F1 to F3 and the Brage East Fault (BEF3) to have been active during the Permian – Early Triassic rifting, based on their hanging-wall wedge-shaped growth packages and the increase in stratigraphic thickness across them, and the Brage East Fault being the dominant fault. The NNW-SSE-striking segment of the Oseberg Fault (OF) was probably mildly active, as suggested by the thickness variations across the fault, along with the significantly larger throw at level T1 than T2 (Fig. 9A). In contrast, the T-z profile of the N-S-striking segment of the Oseberg Fault shows no resolvable T1-T2 activity (Fig. 7). In summary, the active faults or fault segments during the T1-T2 interval strike N-S or NNW-SSE.

5.2. T2 to Intra-Statfjord interval

The most significant increase in thickness for the T2-Intra-Statfjord interval is observed across F9 (100-250 ms TWT or 150-300 m; Fig. 12B). In addition, thickness variations of up to 100 ms TWT (150 m) occur across both the NNW-SSE- and N-S-striking segment of the Oseberg Fault (OF; Fig. 12B). However, no resolvable thickness changes exist across other faults (Fig. 12B).

Minor faults F1-F3 and the Brage East Fault (BEF3) became inactive during the Triassic T2-Intra-Statfjord interval, as shown by Triassic T2-Intra-Statfjord hanging-wall expansion across the faults (Fig. 12B). However, the Oseberg Fault (OF) appears to have been active along the NNW-SSE- and N-S striking segment, but not yet as a continuous fault (Fig. 12B). The F9 was more active than the Oseberg Fault, judging from its larger thickness difference across F9 (Fig. 12B).

5.3. Intra-Statfjord to Top Ness interval

Thickness variations of up to 100 or 100-250 ms TWT (150 or 150-300 m; 1.3-1.5 expansion) are observed across the major faults: the southern segment of the Brage East Fault (BEF3), NNW-SSE- (BF1) and N-S-striking (BF2) segments of the Brage Fault, Oseberg Fault (OF) and F9 (Fig. 12C). Furthermore, thickness changes of <100 ms TWT (150 m; 1.1-1.4 expansion) occur across numerous NW-SW- and N-S-striking minor faults in the southwest of the study area (Fig. 12C). In cross-section, subtle wedge-shaped growth packages develop in the lower part of this unit across the NW-SE-striking minor faults (e.g. F4 in Fig. 7D).

We interpret the N-S- and NNW-SSE-striking segments of the Oseberg Fault to have linked up during this Early – Middle Jurassic time interval as the thickness increase is now also seen in the linkage area between the two segments (Fig. 12C). In addition, stratigraphic thickness variations show that the southern segment (BEF3) of the Brage East Fault and the NNW-SSE- (BF1) and N-S-striking (BF2) segments of the Brage Fault were active (Fig. 12C). For the same reason, a number of NW-SE-striking together with a few N-S-striking minor faults developed (Fig. 12C). Similar to the T2-Intra-Statfjord interval, most of the strain was localized to the NNW-SSE-striking segments of the Oseberg and Brage faults.

5.4. Top Ness to Base Cretaceous Unconformity interval

The Top Ness-Base Cretaceous Unconformity interval are different from the underlying T2-Intra-Statfjord interval in four ways. First, N-S-striking minor faults show thickness changes of up to 100 ms TWT (150 m; 1.2-1.45 expansion) in the southwestern part of the study area (Fig. 12D). Second, thickness changes start to occur across the NE-SW-striking minor faults in the northeast of the study area, mainly less than 100 ms TWT (150m; 1.2-2.0% expansion). Third, the Brage Fault displays a thickness change of >250 ms TWT (300 m; 5.28 expansion) across the central N-S-striking segment (BF2), decreasing laterally to the north and the south. Finally, thickness changes of up to 100 or 100-250 ms TWT (150 m or 150-300 m; 1.4-4.65 expansion) appear across the northern segments (BEF1 and BEF2) of the Brage East Fault (Fig. 12D).

The Top Ness to Base Cretaceous Unconformity interval represents the partly eroded syn-rift 2 package. It is obvious that some of the NW-SE-striking minor faults that formed during the previous interval (see above) remained active during the Middle Jurassic – Early Cretaceous rift phase since they offset the Top Ness horizon (Fig. 4D). However, a few NW-SE-striking minor faults between the NE-SW-striking segment of the Brage Fault and the Oseberg Fault became inactive, such as F3 which terminates in the footwall of the major Oseberg Fault (Fig. 10D).

The southern part of the NE-SW-striking segment of the Brage Fault (BF3), based on the thickness variations, formed during the Middle Jurassic – Early Cretaceous rift phase (Fig. 12D). Similarly, the NE-SW-striking minor faults in the northeast of the study area formed. In addition, the NE-SW-striking segment of the Brage Fault cuts through the T1-T2 growth package and offsets F4, demonstrating that this segment terminated or developed after the active history of F4 (Fig. 7D). The significant thickness increase of this unit in the hanging wall of the Brage Fault indicates that it became the dominant fault during the Middle Jurassic – Early Cretaceous rift phase (Fig. 12D). In comparison to the Intra-Statfjord to Top Ness interval, the main deformation migrated from NW-SE-striking faults to the N-S-striking segment of the Brage Fault (BF2) and NE-SW-striking minor faults during the Middle Jurassic – Early Cretaceous rift phase (Fig. 12D).

6. Discussion

6.1. Fault activity during the inter-rift phase

It is generally assumed that the Middle Triassic – Middle Jurassic inter-rift phase in the northern North Sea was a period of tectonic quiescence and post-rift thermal subsidence (Badley et al., 1988; Færseth, 1996; Odinsen et al., 2000a; Roberts et al., 1993; 1995; Steel, 1993; Yielding et al., 1992). This assumption implies that Permian – Early Triassic faults were tectonically inactive, although thickness change across these faults may still have occurred due to differential compaction over the buried rift topography, particularly in the earliest post-rift stage. However, we found numerous faults that were active during the late stage of the inter-rift phase, especially in the

Intra-Statfjord to Top Ness time interval (Fig. 12C). The Oseberg Fault, for instance, accumulated a throw of up to ~300 ms TWT (~400 m) during the inter-rift phase, equal to that during the Middle Jurassic – Early Cretaceous rift phase (Fig. 9C, 9D). Also, our observations suggest that fault activity was significant and variable during the late stage of the inter-rift phase, with wedge-shaped growth packages in the hanging walls of the NW-SE-trending minor faults (1.1-1.4 expansion; Fig. 10). Such growth packages are not likely to be the result of thermal subsidence alone, and we suggest that the later stage of the inter-rift phase experienced relatively strong tectonic stretching. The newly formed faults during this stage are quite straight in map view and consistently NW-SE-trending, independent of their nearness to pre-existing faults (Fig. 12C). Hence, they seem to be the result of Early Jurassic NE-SW extension.

Ravnås et al. (2000) also called for Middle Triassic – Middle Jurassic inter-rift tectonic activity, and suggested referring to the Middle Triassic – Middle Jurassic succession as inter-rift instead of post-rift. Our work reinforces the model by Ravnås et al. (2000), and shows that fault activity during the interval between the two main phases of rifting was, at least in the Oseberg area, of comparable magnitude to that during the main rift phases.

6.2. Changes in extension direction during multiphase rifting

During the Middle Jurassic – Early Cretaceous rift phase, N-S-, NW-SE- and NE-SW-striking faults were active, suggesting that the extension direction varied temporally and/or laterally during this time interval. The newly formed faults during this interval were N-S-striking in the westernmost part of the Oseberg area (Fig. 12D), but NE-SW-striking in the northeastern part (Fig. 12D). Therefore, the late Jurassic extension direction appears to have been E-W in the western part and NW-SE in the northeastern part of the Oseberg area, assuming that the extension direction is perpendicular to the strike of new-formed faults and that the faults are close to dip slip (Anderson, 1951). However, the dominant Brage Fault, with a N-S strike on average across the area and the main displacement accumulated on its N-S-striking central segment, indicates a general E-W extension direction. While normal faults with different orientations can form simultaneously during none-plane strain (e.g., Healy et al., 2015), crosscutting

relations indicate that the NE-SW-striking segment of the Brage Fault developed later than the N-S- and NW-SE-striking faults (Fig. 7D), which suggests a change in extension direction from E-W to NW-SE during the Middle Jurassic – Early Cretaceous rift phase in this region (Færseth et al., 1997).

Davies et al. (2001) took this view to the extreme, as they suggested that each of several sets of faults in the North Sea rift system are dip-slip normal faults that formed sequentially due to repeated variations in the extension direction, and related these changes to variations in the Middle Jurassic – Early Cretaceous regional extension direction. However, activity on NE-SW-striking fault may be explained by a simple clockwise reorientation of the extension direction in the study area toward NW-SE. Evidence for such a local rotation of the middle-late Jurassic extension is found between the Oseberg and Brage Faults, where the NW-SE-striking minor faults were inactive during the Middle Jurassic – Early Cretaceous rift phase (Fig. 12D). NE-SW-striking faults also developed in the Huldra fault block and Lomre terrace, forming a narrow NE-SW-trending zone that separates the main N-S-striking faults, on both sides (Fig. 1B). Fossen et al. (2003) found the Huldra fault block to be a secondary structure in the middle to late Jurassic rift evolution, related to marginal collapse of the Horda Platform. The zone of NE-SW-trending faults extending from the Oseberg area to the Huldra fault block towards the Lomre and Uer terraces (Fig. 1B) marks the northwestern collapsed margin of the Horda Platform. Seismic evidence for a basement shear zone at this location (Fossen et al., 2016) lead us to speculate that this NE-SW-trending zone is controlled by a basement structural lineament between the Horda Platform and the northern part of Viking Graben, and that activation of this basement structure in the late Jurassic caused the development of the NE-SW-striking faults (also see Færseth, 1996).

In terms of the minor NW-SE-striking faults that were active in the immediate hanging wall of the Oseberg Fault during the Middle Jurassic – Early Cretaceous rift phase (SW part of Fig. 12D), Maerten et al. (2002, 2006) suggested that the curved geometry of the Oseberg and Brage East faults played a great role during the initiation of the NW-SE-striking minor faults. These NW-SE-striking faults are confined to the area

between the Oseberg Fault and the fault to the west, and may possibly be explained as a result of the local, block-internal stress history during the general late Jurassic extension. If so, local stress perturbation by pre-existing first-order structures complicates fault pattern developed during a subsequent rifting phase, varying the strike of new faults around pre-existing structure to be oblique to regional extension direction.

An implication of our study is that fault pattern in multiphase rifts is the result of a combination of far-field stress, basement structures and local perturbations set up by geometry of pre-existing faults. Specifically, basement structures and pre-existing faults lead to variation in the strike of new faults from orthogonal to oblique to the regional far-field stress of rifting. This is consistent with that made from physical modeling of two phases of non-coaxial extension (Henza et al., 2010; 2011), where reactivation of first-phase faults (N-S-striking faults in Fig. 13) and development of new faults (NE-SW-striking faults in Fig. 13) occur during the second-phase extension. In addition, their models show that new faults could strike oblique to the second-phase extension direction due to local perturbations near the reactivated first-phase faults (Fig. 13), similar to the faults developing in the immediate hanging wall of the Oseberg Fault during the Middle Jurassic – Early Cretaceous rift phase (SW part of Fig. 12D). Moreover, many of the second-phase faults cut across or terminate at reactivated first-phase faults, producing intersecting fault geometries in their model that has a well-developed first-phase fault population (Fig. 13), and our results support these conclusions. Therefore, our observations match the conclusions of physical models, and illustrate that basement structures and pre-existing faults play a substantial effect on fault growth during later rift phases.

6.3. Implications for the growth of reactivated pre-existing faults

Several studies have suggested that faults developing by the reactivation of pre-existing faults or intra-crystalline basement weaknesses are prone to establish their final lengths early in their lifespan (Giba et al., 2012; Jackson and Rotevatn, 2013; Paton and Underhill, 2004; Walsh et al., 2002). Our study discovers that renewed growth of pre-existing faults can develop in four different ways. First, a pre-existing

fault gradually propagates upward through the cover after reactivation (Fig. 14A). Second, a pre-existing fault vertically links up with a new fault in the cover (Fig. 14B). Third, a pre-existing fault reactivates and propagates upward into the cover, and is then crosscut by an oppositely dipping fault (Fig. 14C). Finally, the reactivated pre-existing fault terminates against an overlying and oppositely dipping fault (Fig. 14D). The final case may be regarded as an example of what may be a common process, i.e. the restraining or arrest of upward propagating rift faults by an overlying and oppositely dipping fault, associated with the strain shadow of the overlying fault. In fact, the four growth models can happen at various segments of a large fault system, which will lead to irregular, non-elliptical three-dimensional fault geometries. It also implies that fault interactions between faults (e.g. restraining effect in Fig. 14D) can make the reactivation and further growth of a pre-existing fault segmented in the cover, resulting in non-elliptical fault geometries.

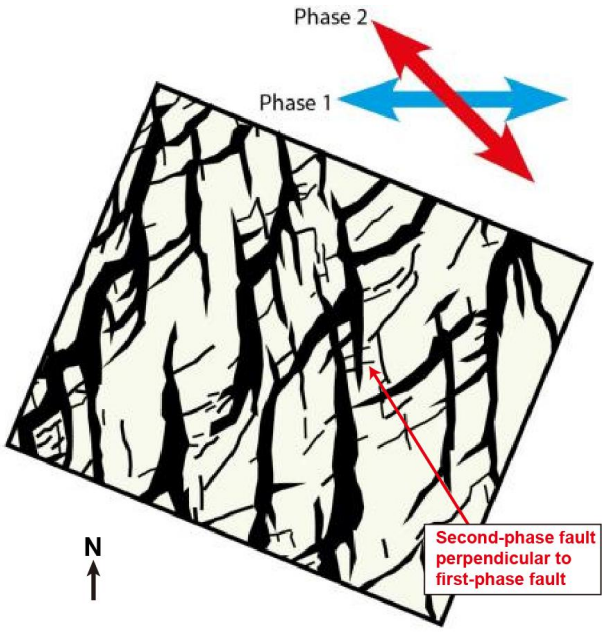

Fig. 13. Fault pattern formed by two phases of non-coaxial extension, based on Henza et al. (2011). Phase 1 extension is E-W (blue arrow), while Phase 2 extension is NW-SE (red arrow), with 45° between the two extension directions. Black line drawings are fault heaves on the top surface of the models.

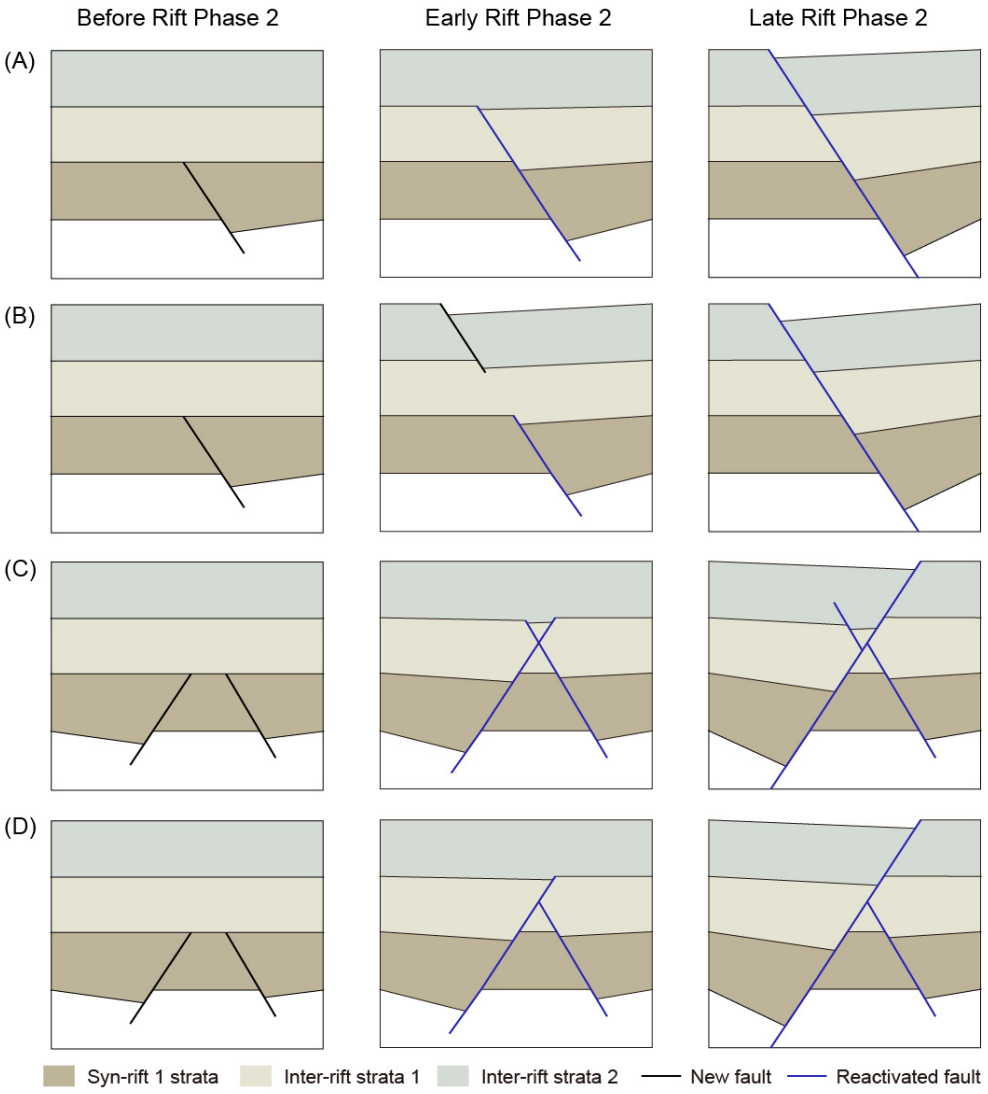

Fig. 14. Four styles of the growth of a reactivated pre-existing fault during a renewed rifting. (A) Upward propagation of a pre-existing fault in the cover during a subsequent rift phase, no influence of other faults. (B) Vertical linkage of a reactivated pre-existing fault and overlying new fault in the cover. (C) Two oppositely dipping faults propagate upward in the cover, followed by one of them crosscutting and offsetting the other. (D) Two oppositely dipping faults propagate upward in the cover, but one of them terminates against the plane or in the footwall block of the other one.

7. Conclusions

1. The evolution of fault array in the Oseberg area can be divided into four stages: (1) the Phase 1 syn-rift period characterized by N-S- and NW-SE-striking, mainly E-dipping faults; (2) early stages of inter-rift evolution, controlled by thermal subsidence and differential compaction; (3) a late inter-rift stage featuring reactivation of Phase 1 faults and formation of NW-SE-striking faults; (4) the Phase 2 syn-rift period resulting in the development of N-S-, NW-SE- and NE-SW-striking faults that are mainly W-dipping.

2. Fault activity is significant during the late inter-rift stage, demonstrating an important Early-Middle Jurassic period of tectonic stretching during the inter-rift phase. Extension direction is NE-SW during the inter-rift phase, rotated clockwise as compared to E-W direction during Phase 1 rifting.

3. Reactivation of pre-existing faults is very significant in the Oseberg area during late inter-rift phase and Phase 2 rifting, indicating that structural inheritance is common during North Sea rifting. Stress perturbation associated with reactivated pre-existing faults changes the strike of new faults to be oblique to the regional stress field.

4. Fault pattern during multiphase rifting is complicated as it is controlled by a combination of far-field stress, basement structures and local perturbations set up by the geometry of pre-existing faults.

5. Upward growth of a reactivated pre-existing structure is influenced by its neighbors in the cover, leading to more non-elliptical fault geometries at the interaction zone.

Acknowledgments

This contribution forms part of the MultiRift Project funded by the Research Council of Norway's PETROMAKS program (Project number 215591) and Statoil to the University of Bergen and partners Imperial College, University of Manchester and University of Oslo. We thank Statoil for providing seismic and well data in this study,

and permission to publish the results of this study. We also thank Rebecca E. Bell, Oliver B. Duffy, Johan S. Claringbould and Antje Lenhart for constructive suggestions regarding the displacement analysis, and Alan Roberts for critically commenting on an earlier version of the manuscript.

Reference

Andersen, T. B. & Jamtveit, B. 1990. Uplift of deep crust during orogenic extensional collapse: a model based on field studies in the Sogn-Sunnfjord region of western Norway. Tectonics 9, 1097-1112.

Anderson, E.M., 1951. The Dynamics of Faulting and Dyke Formation with Applications to Britain. Oliver & Boyd, Edinburgh.

Badley, M., Price, J., Dahl, C.R., Agdestein, T., 1988. The structural evolution of the northern Viking Graben and its bearing upon extensional modes of basin formation. Journal of the Geological Society 145, 455-472.

Badley, M.E., Egeberg, T., Nipen, O., 1984. Development of rift basins illustrated by the structural evolution of the Oseberg feature, Block 30/6, offshore Norway. Journal of the Geological Society 141, 639-649.

Bartholomew, I., Peters, J., Powell, C., 1993. Regional structural evolution of the North Sea: oblique slip and the reactivation of basement lineaments. In: Petroleum Geology Conference Series, 4. Geological Society, London, pp. 1109-1122. Geological Society of London.

Baudon, C., Cartwright, J., 2008a. Early stage evolution of growth faults: 3D seismic insights from the Levant Basin, Eastern Mediterranean. Journal of Structural Geology 30, 888-898.

Baudon, C., Cartwright, J., 2008b. The kinematics of reactivation of normal faults using high resolution throw mapping. Journal of Structural Geology 30, 1072-1084.

Baudon, C., Cartwright, J.A., 2008c. 3D seismic characterisation of an array of blind normal faults in the Levant Basin, Eastern Mediterranean. Journal of Structural Geology 30, 746-760.

Bell, R.E., Jackson, C.A.L., Whipp, P.S., Clements, B., 2014. Strain migration during multiphase extension: Observations from the northern North Sea. Tectonics 33, 1936-1963.

Cartwright, J. A., Trudgill, B. D., & Mansfield, C. S. (1995). Fault growth by segment linkage: an explanation for scatter in maximum displacement and trace length data from the Canyonlands Grabens of SE Utah. Journal of Structural Geology, 17(9), 1319-1326.

Cartwright, J., Bouroullec, R., James, D. & Johnson, H. 1998. Polycyclic motion history of some Gulf Coast growth faults from high-resolution displacement analysis. Geology, 26, 819-822.

Coward, M., Dewey, J., Hempton, M., Holroyd, J., 2003. Tectonic Evolution. The Millennium Atlas: Petroleum Geology of the Central and Northern North Sea, pp. 17-33.

Cowie, P.A., Underhill, J.R., Behn, M.D., Lin, J., Gill, C.E., 2005. Spatio-temporal evolution of strain accumulation derived from multi-scale observations of Late Jurassic rifting in the northern North Sea: A critical test of models for lithospheric extension. Earth and Planetary Science Letters 234, 401-419.

Davies, R., Turner, J., Underhill, J., 2001. Sequential dip-slip fault movement during rifting: a new model for the evolution of the Jurassic trilete North Sea rift system. Petroleum Geoscience 7, 371-388.

Dawers, N. H., & Anders, M. H. (1995). Displacement-length scaling and fault linkage. Journal of Structural Geology, 17(5), 607-614.

Doré, A., Gage, M., 1987. Crustal alignments and sedimentary domains in the evolution of the North Sea, North-east Atlantic Margin and Barents Shelf, Petroleum geology of north west Europe. Graham and Trotman London, pp. 1131-1148.

Dreyer, T., Whitaker, M., Dexter, J., Flesche, H., Larsen, E., 2005. From spit system to tide-dominated delta: integrated reservoir model of the Upper Jurassic Sognefjord Formation on the Troll West Field, Geological Society, London, Petroleum Geology Conference series. Geological Society of London, pp. 423-448.

Duffy, O.B., Bell, R.E., Jackson, C.A., Gawthorpe, R.L., Whipp, P.S., 2015. Fault growth and interactions in a multiphase rift fault network: Horda Platform, Norwegian North Sea. Journal of Structural Geology 80, 99-119.

Færseth, R., 1996. Interaction of Permo-Triassic and Jurassic extensional fault-blocks during the development of the northern North Sea. Journal of the Geological Society 153, 931-944.

Færseth, R.B., Knudsen, B.E., Liljedahl, T., Midbøe, P.S., Søderstrøm, B., 1997. Oblique rifting and sequential faulting in the Jurassic development of the northern North Sea. Journal of Structural Geology 19, 1285-1302.

Færseth, R.B., Ravnas, R., 1998. Evolution of the Oseberg Fault-Block in context of the northern North Sea structural framework. Mar Petrol Geol 15, 467-490.

Fossen, H. (1992). The role of extensional tectonics in the Caledonides of south Norway. Journal of structural geology, 14(8), 1033-1046.

Fossen, H., 1998. Advances tn understanding the post-Caledonian structural evolution of the Bergen area, West Norway.

Fossen, H., Hesthammer, J., Johansen, T. E. S., & Sygnabere, T. O. (2003). Structural geology of the Huldra field, northern North Sea—A major tilted fault block at the eastern edge of the Horda platform. Marine and Petroleum Geology, 20(10), 1105-1118.

Fossen, H., 2010. Extensional tectonics in the North Atlantic Caledonides: a regional view. Geological Society, London, Special Publications 335, 767-793.

Fossen, H., & Rotevatn, A. (2016). Fault linkage and relay structures in extensional settings—A review. Earth-Science Reviews, 154, 14-28.

Frankowicz, E., McClay, K., 2010. Extensional fault segmentation and linkages, Bonaparte Basin, outer North west shelf, Australia. AAPG bulletin 94, 977-1010.

Giba, M., Walsh, J., Nicol, A., 2012. Segmentation and growth of an obliquely reactivated normal fault. Journal of Structural Geology 39, 253-267.

Glennie, K.W., 1987. Outline of North Sea history and structural framework. In: Introduction to the Petroleum Geology of the North Sea, third ed. Blackwell Scientific Publications, Oxford, pp. 34-77.

Gupta, A., & Scholz, C. H. (2000). A model of normal fault interaction based on observations and theory. Journal of Structural Geology, 22(7), 865-879.

Healy, D., Blenkinsop, T. G., Timms, N. E., Meredith, P. G., Mitchell, T. M. & Cooke, M. L. 2015. Polymodal faulting: Time for a new angle on shear failure. Journal of Structural Geology 80, 57-71.

Helland-Hansen, W., Ashton, M., Lømo, L., Steel, R., 1992. Advance and retreat of the Brent delta: recent contributions to the depositional model. Geological Society, London, Special Publications 61, 109-127.

Henza, A.A., Withjack, M.O., Schlische, R.W., 2010. Normal-fault development during two phases of non-coaxial extension: An experimental study. Journal of Structural Geology 32, 1656-1667.

Henza, A.A., Withjack, M.O., Schlische, R.W., 2011. How do the properties of a pre-existing normal-fault population influence fault development during a subsequent phase of extension? Journal of Structural Geology 33, 1312-1324.

Hongxing, G., Anderson, J.K., 2007. Fault throw profile and kinematics of Normal fault: conceptual models and geologic examples. Geol. J. China Univ 13, e88.

Jackson, C.A.-L., Rotevatn, A., 2013. 3D seismic analysis of the structure and evolution of a salt-influenced normal fault zone: a test of competing fault growth models. Journal of Structural Geology 54, 215-234.

Korme, T., Acocella, V., Abebe, B., 2004. The role of pre-existing structures in the origin, propagation and architecture of faults in the Main Ethiopian Rift. Gondwana Research 7, 467-479.

Kyrkjebø, R., Gabrielsen, R., Faleide, J., 2004. Unconformities related to the Jurassic–Cretaceous synrift–post-rift transition of the northern North Sea. Journal of the Geological Society 161, 1-17.

Lepercq, J.-Y., Gaulier, J.-M., 1996. Two-stage rifting in the North Viking Graben area (North Sea): inferences from a new three-dimensional subsidence analysis. Mar. Petroleum Geol. 13, 129-148.

Lepvrier, C., Fournier, M., Bérard, T., Roger, J., 2002. Cenozoic extension in coastal Dhofar (southern Oman): implications on the oblique rifting of the Gulf of Aden. Tectonophysics 357, 279-293.

Lervik, K., 2006. Triassic lithostratigraphy of the northern North Sea Basin. Norsk Geologisk Tidsskrift 86, 93.

Long, J., Imber, J., 2010. Geometrically coherent continuous deformation in the volume surrounding a seismically imaged normal fault-array. Journal of Structural Geology 32, 222-234.

Maerten, L., Gillespie, P., & Pollard, D. D. (2002). Effects of local stress perturbation on secondary fault development. Journal of Structural Geology, 24(1), 145-153.

Maerten, L., Gillespie, P. & Daniel, J.-M. 2006. Three-dimensional geomechanical modeling for constraint of subseismic fault simulation. American Association of Petroleum Geologists Bulletin 90, 1337-1358.

Nixon, C. W., Sanderson, D. J., Dee, S. J., Bull, J. M., Humphreys, R. J., & Swanson, M. H. (2014). Fault interactions and reactivation within a normal-fault network at Milne Point, Alaska. AAPG Bulletin, 98(10), 2081-2107.

Odinsen, T., Christiansson, P., Gabrielsen, R.H., Faleide, J.I., Berge, A.M., 2000a. The geometries and deep structure of the northern North Sea rift system. Geological Society, London, Special Publications 167, 41-57.

Odinsen, T., Reemst, P., Beek, P.V.D., Faleide, J.I., Gabrielsen, R.H., 2000b. Permo-Triassic and Jurassic extension in the northern North Sea: results from tectonostratigraphic forward modelling. Geological Society, London, Special Publications 167, 83-103.

Paton, D.A., Underhill, J.R., 2004. Role of crustal anisotropy in modifying the structural and sedimentological evolution of extensional basins: the Gamtoos Basin, South Africa. Basin Research 16, 339-359.

Peacock, D., Sanderson, D., 1991. Displacements, segment linkage and relay ramps in normal fault zones. Journal of Structural Geology 13, 721-733.

Ravnås, R., Nøttvedt, A., Steel, R.J., Windelstad, J., 2000. Syn-rift sedimentary architectures in the Northern North Sea. Geological Society, London, Special Publications 167, 133-177.

Roberts, A., Yielding, G., Badley, M., 1990. A kinematic model for the orthogonal opening of the Late Jurassic North Sea rift system, Denmark-Mid Norway. Tectonic Evolution of the North Sea Rifts, Clarendon Press, Oxford, 180-199.

Roberts, A., Yielding, G., Kusznir, N., Walker, I., Dorn-Lopez, D., 1993. Mesozoic extension in the North Sea: constraints from flexural backstripping, forward modelling and fault populations, Geological Society, London, Petroleum Geology Conference series. Geological Society of London, pp. 1123-1136.

Roberts, A., Yielding, G., Kusznir, N., Walker, I., Dorn-Lopez, D., 1995. Quantitative analysis of Triassic extension in the northern Viking Graben. Journal of the Geological Society 152, 15-26.

Smethurst, M., 2000. Landeoffshore tectonic links in western Norway and the northern North Sea. J. Geol. Soc. 157, 769-781.

Steel, R., 1993. Triassic–Jurassic megasequence stratigraphy in the Northern North Sea: rift to post-rift evolution, Geological Society, London, Petroleum Geology Conference series. Geological Society of London, pp. 299-315.

Steel, R., Ryseth, A., 1990. The Triassic—Early Jurassic succession in the northern North Sea: megasequence stratigraphy and intra-Triassic tectonics. Geological Society, London, Special Publications 55, 139-168.

Stewart, I.J., Rattey, R.P., Vann, I.R., 1992. Structural style and the habit of hydrocarbons in the North Sea. In: Larsen, R.M., Brekke, H., Larsen, B.T., Talleraas, E. (Eds.), Structural and Tectonic Modelling and its Application to Petroleum Geology, 1. NPF Spec. Publ, pp. 197-220.

Ter Voorde, M., Faerseth, R.B., Gabrielsen, R.H., Cloetingh, S.A.P.L., 2000. Repeated lithosphere extension in the northern Viking Graben: a coupled or a decoupled rheology? Geological Society, London, Special Publications 167, 59-81.

Tomasso, M., Underhill, J.R., Hodgkinson, R.A., Young, M.J., 2008. Structural styles and depositional architecture in the Triassic of the Ninian and Alwyn North fields: Implications for basin development and prospectivity in the Northern North Sea. Mar Petrol Geol 25, 588-605.

Underhill, J.R., Partington, M.A., 1993. Jurassic thermal doming and deflation in the North Sea: implications of the sequence stratigraphic evidence. Geol. Soc. Lond. 4, 337-345.

Vetti, V. V., & Fossen, H. (2012). Origin of contrasting Devonian supradetachment basin types in the Scandinavian Caledonides. Geology, 40(6), 571-574.

Walsh, J., Nicol, A., Childs, C., 2002. An alternative model for the growth of faults. Journal of Structural Geology 24, 1669-1675.

Walsh, J.J., Watterson, J., 1991. Geometric and kinematic coherence and scale effects in normal fault systems. In: Geological Society, London, Special Publications, vol. 56, pp. 193-203.

Whipp, P., Jackson, C., Gawthorpe, R., Dreyer, T., Quinn, D., 2014. Normal fault array evolution above a reactivated rift fabric; a subsurface example from the northern Horda Platform, Norwegian North Sea. Basin Research 26, 523-549.

Yielding, G., Badley, M.E., Roberts, A.M., 1992. The structural evolution of the Brent Province. Geological Society, London, Special Publications 61, 27-43.

Young, M.J., Gawthorpe, R.L., Hardy, S., 2001. Growth and linkage of a segmented normal fault zone; the Late Jurassic Murchison–Statfjord North Fault, northern North Sea. Journal of Structural Geology 23, 1933-1952.

Ziegler, P., 1992. North Sea rift system. Tectonophysics 208, 55-75.

Ziegler, P.A., 1990. Tectonic and Palaeogeographic Development of the North Sea Rift System. Tectonic Evolution of the North Sea Rifts. Clarendon Press, Oxford, pp. 1-36.

SYNTHESIS

This thesis aims to understand how a pre-existing structure or weakness reactivates and influences the fault growth and final fault network in three dimensions during a secondary phase of rifting, via interpretation of seismic data (Paper I) and the results of some generic discrete element modeling (Papers II & III). Paper I focuses on the final fault geometry and the interpretation of fault network evolution of the Oseberg area in the norther North Sea rift over the Permian – Early Triassic and Middle Jurassic – Early Cretaceous rift phases. Papers II and III show the results of discrete element modeling and examine the variation in the final fault geometry and fault network, and their evolution over a weak planar pre-existing structure during extension owing to the difference in the orientation relative to the extension direction and the dip of the pre-existing structure. The results of the thesis provide some new insights on the reactivation pattern of pre-existing structures, and the fault network and fault growth history affected by pre-existing structures during rifting.

The significance of inter-rift activity between two rift phases

This research demonstrates that fault activity is common and systematically distributed during the inter-rift phase in the study area, as opposed to the general view that this stage is dictated by post-rift thermal subsidence. Based on our research, the evolution of the Oseberg fault array comprises: (i) the Permian – Early Triassic rift phase which is characterized by N-S- and NW-SE-striking, mainly E-dipping faults; (ii) early stages of inter-rift evolution, controlled by thermal subsidence and differential compaction; (iii) a late inter-rift stage featuring reactivation of Permian – Early Triassic faults and formation of NW-SE-striking faults; and (iv) the Middle Jurassic – Early Cretaceous rift phase resulting in the concurrent development of the N-S-, NW-SE- and NE-SW-striking faults that are mainly W-dipping. The Permian – Early Triassic faults are mainly N-S-striking, resulting from E-W extension. Fault activity is significant during the late inter-rift stage, demonstrating an important Early – Middle Jurassic period of

tectonic stretching during the inter-rift phase. Extension is NE-SW during the inter-rift phase, as indicated by the NW-SE-trending faults. Hence, there is clockwise rotation as compared to the E-W Permian – Early Triassic extension. During the Middle Jurassic – Early Cretaceous rift phase, the extension direction appears to rotate back to the E-W direction as indicated by the formation of N-S oriented major faults during this time period. These observations suggest a reorientation of the stress field from E-W during the Permian – Early Triassic rift phase to NE-SW during inter-rift fault growth and back to E-W during the Middle Jurassic – Early Cretaceous rift phase in the Oseberg area. In addition, fault pattern during multiphase rifting is complicated as it is controlled by a combination of far-field stress, basement structures and local perturbations set up by the geometry of pre-existing faults.

How variable is the reactivation pattern of a pre-exiting structure associated with a change in its orientation relative to the extension direction and the dip?

The reactivation of pre-existing faults or structures were recorded extensively in rift basins (e.g., Badley et al., 1988; Færseth, 1996; Odinsen et al., 2000; Lepvrier et al., 2002; Morley et al., 2004; Frankowicz and McClay, 2010; Nixon et al., 2014; Whipp et al., 2014; Duffy et al., 2015). These studies mainly investigated the fault geometries and evolution of fault network based on interpretation of subsurface or field data, and showed that pre-existing faults or structures commonly reactivate and interact with newly formed faults during a later rift phase (e.g., Færseth, 1996; Lepercq and Gaulier, 1996; Morley et al., 2004; Morley, 2007; Frankowicz and McClay, 2010; Bell et al., 2014; Nixon et al., 2014; Whipp et al., 2014; Duffy et al., 2015). For example, Whipp et al. (2014) suggested the control of structural inheritance of Pre-Jurassic faults on the fault array during the Middle Jurassic – Early Cretaceous rift phase in the Horda Platform in the northern North Sea. Duffy et al. (2015) made a further analysis on the three-dimensional geometries of the fault array and the styles of fault interactions in this region and emphasized the effect of the reactivation of Pre-Jurassic major faults on the development of small Jurassic faults. Similarly, Morley et al. (2004) highlighted the influence of pre-existing structural fabrics on the rift development in the Thailand

Rift and suggested that the well-developed fabric inherited from Palaeozoic and Mesozoic orogenies exerted a strong influence on the orientation and geometry of Tertiary faults. Also, Frankowicz and McClay (2010) identified three major populations of extensional faults of different ages and interpreted that the youngest population was inherited from the underlying zones of weakness. In contrast, there are also observations that pre-existing faults or structures can remain inactive during a later rift phase. For example, Pre-Jurassic faults were crosscut and offset by Middle Jurassic – Early Cretaceous faults in the East Shetland Basin in the northern North Sea, suggesting that pre-existing faults or structures are not necessarily reactivated during a later rift phase (e.g., Badley et al., 1988; Yielding et al., 1992; Nøttvedt et al., 1995; Roberts et al., 1995; Færseth, 1996; Odinsen et al., 2000; Tomasso et al., 2008). Uncertainty still exits on the nature of the reactivation of pre-existing structures or faults during an extension phase.

Etheridge (1986) suggested that reactivation of a pre-existing structure of fault will depend primarily on the relative strength the pre-existing structure to the host rock, and the orientation in the prevailing stress field. The strength of the pre-existing structure is associated with fault gouge, mineral, depth, fluid etc. The study of Ivins et al. (1990) indicated that any reduction in frictional strength (e.g., enhanced fluid pore pressure) of the pre-existing structure below that of surrounding rock increases the likelihood that such structures will be first breaking. In terms of orientation, a pre-existing structure optimally oriented relative to the extension direction is more likely to be reactivated (e.g., Bonini et al., 1997; Dubois et al., 2002; Bellahsen and Daniel, 2005; Henza et al., 2010, 2011). Henza et al., (2010, 2011) used a set of wet clay models to simulate two phases of non-coaxial extension with various angles (up to 45°) between the extension directions, indicating that first-phase faults can be reactivated during the second phase of extension in all the models, with the number and length of reactivated first-phase faults decreasing as the angle increases. However, those physical analog models are restricted to fault array on the top surface of the models.

The reactivation pattern and geometry of a pre-existing fault system in three dimensions is poorly understood.

This study employs the numerical modeling method and examines the reactivation pattern of a weak planar pre-existing structure in three dimensions during an orthogonal or oblique extension (Paper III). Our modeling results show that the reactivation pattern associated with a weak planar pre-existing structure is variable with respect to the different strike angle relative to the extension direction and the dip of the pre-existing structure. In detail, a pre-existing structure can either fully reactivate and finally become a big, major fault, or partly reactivate as a few segments that individually link up with other new faults nucleating away from the pre-existing structure, or even remain inactive during extension. Our study first documents the variation in the reactivation pattern of a pre-existing structure in three dimensions associated with its strike angle relative to the extension direction and the dip, which contributes to understanding the reactivation pattern of a pre-existing structure in natural rifts.

How does a reactivated structure grow in three dimensions during an extension?

It is accepted that normal fault growth follows one or a combination of the two end-member models: (i) the isolated fault model (e.g., Walsh and Watterson, 1988; Trudgill and Cartwright, 1994; Dawers and Anders, 1995; Cartwright et al., 1995; Schische and Anders, 1996; Kim and Sanderson, 2005; Baudon and Cartwright 2008); or (ii) the coherent fault model (e.g., Childs et al., 1995; Walsh et al., 2002, 2003; Schöpfer et al., 2006, 2007; Giba et al., 2012). The isolated fault model suggests that a normal fault system develop from the initiation of a few small, isolated fault segments, which then grow, link and amalgamate to form a larger, through-going fault (Cartwright et al., 1995; Gawthorpe and Leeder, 2000; Gawthorpe et al., 1997; Mansfield and Cartwright, 2001; Peacock and Sanderson, 1991). The coherent fault model, on the other hand, implees that fault segments splay vertically or laterally from a single fault surface, with each fault segment initiating as a component of a spatially and mechanically related array (e.g., Childs et al., 1995; Walsh et al., 2002, 2003;

Schöpfer et al., 2006, 2007; Giba et al., 2012). Walsh et al. (2002) proposed that the coherent fault model could better explain the reactivation of pre-existing structures and that reactivated pre-existing structures rapidly obtain their final length, followed by a long period of displacement accruement.

The growth of pre-existing structures in our discrete element modeling has is consistent with the coherent fault model, and our result provide new knowledge about fault growth and interaction of pre-existing structures in three dimensions. For example, the growth of a pre-existing structure oblique ($\alpha \geq 60°$ and $\beta = 60°$) to the extension direction can be summarized in three stages: (i) reactivation of the pre-existing structure and nucleation of new faults; (ii) radial propagation and interaction of the reactivated structure and new faults; and (iii) linkage of the reactivated structure and adjacent faults and formation of non-planar faults (Paper II). From our modeling results, the pre-existing structure reactivates and ruptures along its length very quickly during the first 10% of extension, reaching a long, highly under-displaced fault that is dominated by displacement accumulation in the remaining period of the growth history. This is consistent with the coherent fault model of Walsh et al. (2002) where pre-existing structures rapidly obtain their final length, followed by a long period of displacement accruement. In addition, the reactivated structure propagates upward by means of a few 'saw-tooth' fringes that resemble the kinematically related segments of a fault array in the coherent model (Child et al. 1995, 1996). Hence, we clarify the detailed geometry and growth history of pre-existing structures and demonstrate the upward growth of pre-existing structures via some 'saw-tooth' fringes or kinematically related fault segments arising from the upper tip of pre-existing structures.

How does a reactivated structure impact the nearby fault network?

Morley et al. (2004) investigated rift-related faults affected by well-developed fault fabric inherited from Paleozoic and Mesozoic orogenies in the Tertiary rift basins of Thailand and suggested that normal fault systems are influenced in a number of ways

by oblique pre-existing fabrics: these include (i) oblique orientation of faults, (ii) preferred main fault and splay orientations oblique to the regional extension direction, (iii) the location, geometry and style of transfer zones, and (iv) fault linkage and displacement patterns. Henza et al. (2010) suggested that reactivated first-phase faults can influence the length, number, orientation and location of second-phase faults by physical analog models. Our study focuses on understanding the effect of a single pre-existing structure on the nearby fault network with different strike angles relative to the extension direction and the dips of the pre-existing structure. According to our modeling results, a favorably oriented pre-existing structure influences the adjacent fault network by changing the (i) fault density, (ii) length, (iii) orientation and, (iv) displacement and by providing favorable sites for (v) fault nucleation.

What does the effect of a pre-existing structure on adjacent new faults imply?

The isolated fault model assumes that an isolated normal fault commonly grows by radial propagation, with the displacement maximum to be found in the middle of the fault, from where the displacement decreases towards the tips (e.g., Walsh and Watterson, 1988; Cowie and Scholz, 1992; Peacock and Sanderson, 1992; Dawers and Anders, 1993). Along-strike displacement variations with several locations of displacement maximum can be a result of the linkage of several smaller fault segments. The linkage area commonly has a displacement minimum showing the former tip of segments (e.g., Peacock and Sanderson, 1996; Peacock, 2002). This forms the basis of interpreting fault growth history by analyzing final displacement distribution or D-L relations. However, our study questions this basis as the location of the final displacement maximum of a fault segment is not necessary its nucleation point. The location of displacement maximum may change during the deformation history related to displacement enhancement at the linkage area with a reactivated major structure.

Future work

This study investigates the structural evolution and the growth histories of pre-existing structures in the Oseberg area in the northern North Sea from Permian to Early Cretaceous (Paper I). The reactivation pattern and growth history of a pre-existing structure is further studied in three dimensions by using discrete element modeling, with a focus on how a pre-existing structure influence the nearby fault network during extension (Paper II and III). Using this research as a starting point, some further work can be carried out to increase our understanding of fault growth affected by pre-existing structures during rift development.

The first step is to make an effort to disclose more information about pre-rift structures or intra-basement structures that are associated with the subsequent development of normal faults in rift basins, such as the geometry, distribution, if possible, the strength of pre-existing structures. My study is limited to the quality of the seismic data in depth, making it challenging to map the basement and intra-basement structures across the study area. However, analysis of these structures can not only improve the current knowledge about the linkage between pre-existing structures and subsequent rift development, but also justify the results obtained from physical and numerical models. In return, the modeling results presented in this research provide an insight of the effect of pre-existing structures on the fault growth during a later rift phase, which is of great help for the interpretation of seismic data and understanding of structural features in rift development. The combination of natural examples and modeling results will make the investigation of normal fault growth in rifts more feasible. Hence, investigation on the features of pre-existing structures in detail will benefit the understanding of rift development.

The modeling results presented in this study demonstrate that discrete element modeling is a very useful technique for studying crustal deformation. In particular, this technique can provide valuable predictions of fault growth and rift evolution, which is beneficial for understanding the three-dimensional fault geometries and their evolution during extension. However, our models have only one single pre-existing structure,

giving some generic examples for understanding the theoretical process of the effect of a pre-existing structure on fault growth during extension. Future work can aim to establish some more complex models by increasing the number of pre-existing structures and arranging them in specific patterns according to the observations from natural examples, trying to explain the formation of those structural features by numerical modeling.